6.08
Tracers of Ocean Mixing

W. J. Jenkins

Woods Hole Oceanographic Institution, MA, USA

6.08.1 INTRODUCTION

The distributions of chemicals within the ocean are governed by a variety of biological, chemical, physical, and geological processes. The relative importance of each process in controlling a geochemical element's distribution varies from substance to substance, depending on its chemical reactivity and role in various biogeochemical cycles. Often, these processes are poorly understood and inextricably intertwined. Consider, for example, the distribution of dissolved oxygen in the Atlantic (Figure 1).

Oxygen is driven toward saturation on contact with the atmosphere, produced by biological fixation in the upper ocean, and consumed by bacterial degradation of organic material in the water column and sediments below. These processes are clearly variable in both space and time, and are not well quantified. In addition to these biogeochemical processes, one sees the effects of large-scale circulation, ventilation, and mixing on its distribution. Note, for example, the penetration of high-oxygen water into the abyss from the north, and into intermediate depths from the south. Since the large-scale dissolved oxygen distribution appears to be in approximate steady state, it must represent a balance between both physical and biogeochemical processes.

Physical processes, however, are a common determinant for the distributions of all geochemical distributions, and their quantification may lead to insight into the magnitude aznd nature of the other processes. For example, determination of tracer ventilation rates has been used to quantify oxygen utilization rates, which in turn can be used to estimate export production in the ocean (Jenkins, 1984; Jenkins and Wallace, 1992).

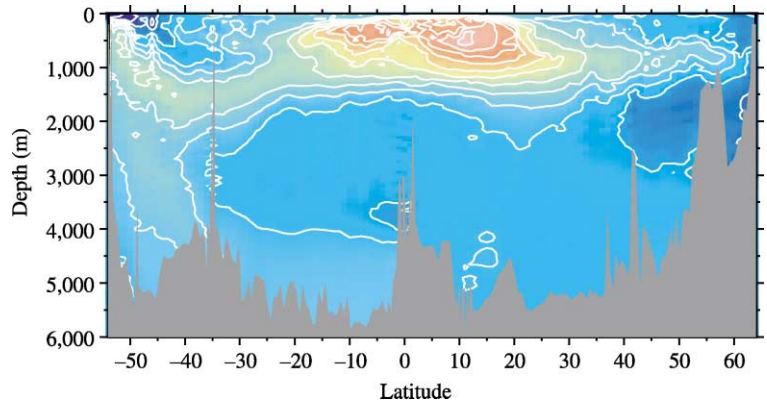

Figure 1 The meridional distribution of dissolved oxygen in the central Atlantic. Blue corresponds to high concentrations and red to low.

Conversely, the distributions of some geochemicals whose biogeochemical behaviors are well understood or sufficiently simple may be used to obtain quantitative information regarding the magnitude of physical processes in the ocean.

Fluid flow in the oceans is generally turbulent. This turbulence occurs on space scales ranging from millimeters to hundreds of kilometers, and in concert with convection and molecular diffusion, works to homogenize properties within the ocean. Nevertheless, the oceans are *not* homogeneous because large-scale processes that change seawater properties are at work both in the ocean interior (e.g., particle sinking, see Chapter 6.09) and at the oceanic boundary layers, where they contact the atmosphere and the solid earth. The resultant distributions arise from an approximate balance between this "biogeochemical and boundary forcing" and ocean ventilation, circulation, and mixing. The nature and magnitude of these physical processes are crucial in determining the oceanic physical and biogeochemical states, and how they will evolve in the face of global change.

Since the ocean is a key element in the climate system, global-scale ocean models play a central role in climate change forecasting, from the viewpoint of both heat transport and carbon dioxide uptake and sequestration. These models are used to predict the shift in the biogeochemical state of the ocean due to direct anthropogenic impact and changes in climate forcing. Although becoming increasingly sophisticated and powerful, such models are necessarily idealized. This arises from the fact that physical processes occur on space scales spanning more than 18 orders of magnitude (from molecular to planetary scale), whereas we are presently computationally limited to a mere 3 or 4 orders of magnitude. Subgridscale processes, i.e., processes occurring on spatial and temporal scales not actually resolved by the models, must be represented by some integrated quasi-statistical parametrization. Mixing is a key example of such processes. The magnitude and, indeed, the nature of the parametrization can be (and have been) estimated heuristically, but ultimately, the magnitude and validity of this parametrization is rooted in oceanic observations.

Tracers represent a potent tool in this regard. Tracers constitute a general class of materials in the ocean that occur in sufficiently small quantities (they are *trace*) that they do not directly influence the fluid's density and hence behavior. (Temperature and salinity have been referred to as "active" tracers (as opposed to the other "passive" tracers), and technically do not fall within this strict definition.) More importantly, however, is the fact that they *trace* fluid flow in some fashion. An example of this is the penetration of bomb-produced tritium into the North Atlantic (Figure 2), which traces the entry point of newly ventilated water into the global overturning circulation. In a qualitative sense, such distributions provide compelling visualizations of ventilation pathways and timescales of the circulation simply by showing where the tracer *is* and where the tracer *is not*. Presence of a bomb-produced tracer at a location in the abyssal Atlantic in the 1980s, for example, implies a connection to the ocean surface within the past few decades. Comparing Figures 1 and 2, for example, leads one to infer the importance and rates of ventilation pathways in determining the distribution of oxygen in the deep North Atlantic.

Tracers integrate over space- and timescales processes that occur in a patchy and often episodic fashion. Thus, they provide space- and time-averaged information on these processes, often on scales that are relevant to important oceanographic and climate problems. These attributes, however, prove to be significant challenges as well. The manner in which a tracer integrates these processes is intrinsically colored by the

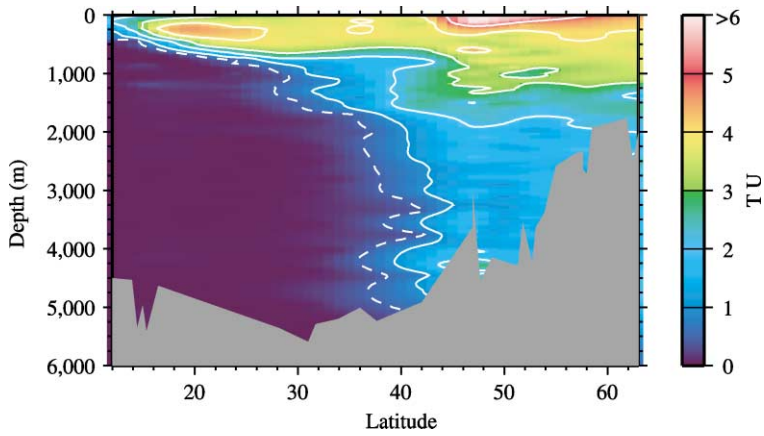

Figure 2 The meridional distribution of tritium in the central North Atlantic in the early 1980s.

nature of the tracer, its reactivity (if any), boundary conditions, and time history (if transient) (e.g., see Doney and Jenkins, 1988). These aspects may not be perfectly known, and the actual observational database tends to be more sparse or noisy than desired. Moreover, the information extracted from the observed tracer distributions is in general model dependent. Different tracers, however, tend to illuminate different aspects of biogeochemical and physical processes, so that combining these different observations provides stronger constraints than from individual tracers. An analogy might be observing a scene through a single color filter: the basic features of the scene are revealed, but adding color components builds a clearer, more complete picture, because each component adds new and unique features to the scene.

The objective of this chapter is to provide an overview of recent advances in the use of tracers to measure ocean mixing, circulation, and ventilation. This is an extremely broad and active area of research, so the discussion will be by no means comprehensive. Rather than providing a litany encompassing everything that has been published in the past few decades on tracers and ocean mixing, I will attempt to discuss a small number of recent studies within a simplified theoretical framework. The hope is that this will provide the reader with a better synthesis of where the field stands as of early 2000s, and where significant advances are likely to occur. The discussion will not include tracers that are dominated by processes such as sorption/desorption in the marine environment (e.g., particle reactive tracers; see Chapter 6.09), and will not dwell on large-scale modeling efforts (whether prognostic or inverse), although each are of considerable importance in marine geochemistry.

To set the stage for a discussion of current work on using tracers to study mixing, I begin in the next section by discussing the basic theory behind advection–diffusion modeling. This is followed in Section 6.08.3 with a brief characterization of mixing in the ocean. The following two sections (Sections 6.08.4 and 6.08.5) are an outline some of the recently developed framework theory for discussing tracer results. These will be followed with a brief overview of steady-state tracers (Section 6.08.6), and a more in-depth discussion of transient tracers (Section 6.08.7). Section 6.08.8 is a discussion of age tracer techniques, and Section 6.08.9 treats purposeful tracer release experiments. A final section includes some concluding remarks and some speculation about the future.

6.08.2 THEORETICAL FRAMEWORK 1: THE ADVECTION–DIFFUSION EQUATION

We shall consider the distribution of a scalar property C in one dimension for simplicity. It can be described by an advection–diffusion relationship

$$\frac{\partial C}{\partial t} + \frac{\partial}{\partial x}(uC) = D\frac{\partial^2 C}{\partial x^2} + J \qquad (1)$$

where D is the molecular diffusivity, u is the fluid velocity, and J is an *in situ* source/sink term. In a turbulent-fluid environment, there exist random fluctuations in fluid velocity and scalar concentrations that can be described in terms of mean and fluctuating components:

$$u = \bar{u} + u', \qquad C = \bar{C} + C' \qquad (2)$$

where

$$\bar{u} = \frac{1}{T}\int_T u\,\mathrm{d}t, \qquad \bar{C} = \frac{1}{T}\int_T C\,\mathrm{d}t \qquad (3)$$

where T is an appropriate averaging timescale. Thus, by definition

$$\int_T u' \, dt = 0, \qquad \int_T C' \, dt = 0 \tag{4}$$

The assumption is that there exists some timescale that allows us to separate the random fluctuations from the mean (e.g., see Tennekes and Lumley, 1972). That is, there exists some meaningful average for these properties. Substituting these definitions into Equation (1), integrating over T, and utilizing Equations (4) to eliminate terms, we obtain

$$\frac{\partial \bar{C}}{\partial t} + \frac{\partial}{\partial x}(\bar{u}\bar{C} + \overline{(u'C')}) = D\frac{\partial^2 \bar{C}}{\partial x^2} + J \tag{5}$$

where the overbar represents integration over the interval T. The resultant equation resembles the original Equation (1) except for the averaged product of the fluctuations, which is called the *Reynolds flux*. If the fluid and concentration fluctuations were uncorrelated, then this term would integrate to zero, but in practice there is a correlation, because there is likely a causal relationship between fluid motion and concentration fluctuations. By assuming that concentration fluctuations are caused by random fluid parcel displacements of length l' in a macroscopic concentration gradient (e.g., see Garrett, 1989), we can reformulate the Reynolds flux term

$$\frac{\partial \bar{C}}{\partial t} + \frac{\partial}{\partial x}\left(\bar{u}\bar{C} - \overline{u'l'}\frac{\partial \bar{C}}{\partial x}\right) = D\frac{\partial^2 \bar{C}}{\partial x^2} + J \tag{6}$$

Here, the putative length scale represents some kind of mean displacement, or some Lagrangian decorrelation scale that is evidenced by a granularity in the tracer distribution (see Armi and Stommel, 1983; Jenkins, 1987; Joyce and Jenkins, 1993). The $\overline{u'l'}$ term is usually characterized as a turbulent diffusion coefficient κ, because of its functional similarity to the molecular diffusion coefficient:

$$\frac{\partial C}{\partial t} + \frac{\partial}{\partial x}(uC) = D\frac{\partial^2 C}{\partial x^2} + \frac{\partial}{\partial x}\left(\kappa\frac{\partial C}{\partial x}\right) + J \tag{7}$$

At this point, the variables C and u are now used to connote the average (macroscopic) tracer concentration and velocity, respectively, and the overbar is dropped for convenience. Implicit in this formulation is the belief that fundamentally Lagrangian (particle) dispersion can be modeled as a continuum Eulerian phenomenon in a fashion analogous to the Fickian formulation of molecular transport by Brownian motion. This is a useful fiction for simple modeling exercises, but must be used with caution (see the next section on isopycnal diffusion).

Expanding the turbulent diffusion term, one obtains an additional pseudo-advective term:

$$\frac{\partial C}{\partial t} + \frac{\partial}{\partial x}(uC) = D\frac{\partial^2 C}{\partial x^2} + \frac{\partial \kappa}{\partial x}\left(\frac{\partial C}{\partial x}\right) + \kappa\frac{\partial^2 C}{\partial x^2} + J \tag{8}$$

which should be accounted for in regions of strong eddy kinetic energy gradients (and hence changing mixing rates) since it behaves like a velocity (e.g., see Armi, 1979). If κ is assumed to be spatially invariant Equation (7) can be reduced to a simpler form

$$\frac{\partial C}{\partial t} + \frac{\partial}{\partial x}(uC) = (D + \kappa)\frac{\partial^2 C}{\partial x^2} + J \tag{9}$$

Now it will become evident that for most oceanic circumstances $\kappa \gg D$, usually by several orders of magnitude, so that the molecular diffusivity can be safely ignored, giving the familiar time-dependent advection–diffusion equation

$$\frac{\partial C}{\partial t} + \frac{\partial}{\partial x}(uC) = \kappa\frac{\partial^2 C}{\partial x^2} + J \tag{10}$$

An important characteristic of a property distribution is encapsulated in the *Peclet number*, $Pe = UL/\kappa$, which is the ratio of diffusive timescale to advective timescale of the system. In this definition, U and L are the characteristic velocity and length scales of the flow. The Peclet number is a measure of the relative importance of advection *versus* diffusion, where a large number indicates an advectively dominated distribution, and a small number indicates a diffuse flow. Numerical modeling indicates that certain tracer distributions, in particular tracer–tracer relationships, are significantly affected by the Peclet number, and consequently can be used to determine the nature of the fluid flow (Jenkins, 1988; Musgrave, 1985, 1990).

Equation (10) can be expressed in three dimensions as

$$\frac{\partial C}{\partial t} = \kappa\nabla^2 C - \vec{u}\cdot\nabla C + J \tag{11}$$

where κ now becomes an anisotropic eddy diffusivity tensor. Since buoyancy forces suppress fluid motion in a direction orthogonal to isopycnal surfaces (or more properly, neutral surfaces McDougall, 1987), which tends to be approximately vertical, terms associated with that direction are much smaller than horizontal. To the extent that such surfaces exhibit slope in response to horizontal pressure gradients (largely but not solely geostrophic in nature), there will be off-diagonal terms in the diffusivity tensor if expressed in "geodesic" coordinates (Redi, 1982). Expressing the tracer balance in a more "natural" density (isopycnal) coordinate system

(where the x- and y-directions are aligned with the isopycnal, and the "z"-direction is orthogonal) effectively diagonalizes the diffusivity tensor

$$\frac{\partial C}{\partial t} = \kappa_\rho \nabla_\rho^2 C - \vec{u} \cdot \nabla_\rho C + J \qquad (12)$$

where the subscript ρ indicates operation in the density coordinate space.

Equation (12), when used in large-scale coarse resolution (non-eddy resolving) models, is incomplete in one other respect. The effect of mesoscale eddies on tracer transport includes an additional, advective-like mechanism sometimes referred to as "bolus transport" (see Gent and McWilliams, 1990; Gent *et al*., 1995). This can be included in Equation (12) as

$$\frac{\partial C}{\partial t} = \kappa_\rho \nabla_\rho^2 C - \left(\vec{u} + \frac{\overline{h'_\rho u'}}{\overline{h_\rho}} \right) \cdot \nabla_\rho C + J \qquad (13)$$

where h_ρ is the isopycnal layer thickness. This underlines an important limitation to the turbulent diffusion concept: it is an Eulerian continuum approximation to a fundamentally Lagrangian process. In subsequent discussion, this factor will be ignored, but it is of fundamental importance in large-scale numerical modeling.

A final modification to these equations is necessary if the substance under consideration is radioactive, or subject to some first-order concentration-dependent consumption or removal process. Thus in general (11) can be rewritten as

$$\frac{\partial C}{\partial t} = \kappa \nabla^2 C - \vec{u} \cdot \nabla C - \lambda C + J \qquad (14)$$

Within the framework of this equation, tracers may be broadly categorized as

- *conservative* ($J = 0$) or *nonconservative*, counterexamples being dissolved atmospheric argon *versus* dissolved oxygen;
- *steady state* ($\partial C/\partial t = 0$) or *transient*, counterexamples being silica *versus* bomb produced tritium;
- *stable* ($\lambda = 0$) or *radioactive*, counterexamples being dissolved atmospheric helium *versus* radon; and
- *passive* (nondensity affecting) or *active*, counterexamples being CFC-11 *versus* temperature or salinity.

This classification has been discussed extensively within the context of a one-dimensional advection–diffusion model, along with simple solutions to the relevant equations (Craig, 1969). It should be noted, however, that specific tracers may fall into different categories depending on the nature of the specific application. For example, radiocarbon is a transient tracer in the surface waters of the ocean because its natural inventory (due to cosmic ray production) has been affected both by dilution with fossil fuel carbon and by massive production from atmospheric nuclear weapons testing. In deep Pacific ocean waters, however, it is more a steady-state tracer (see Section 6.08.6). Moreover, there are regions of the ocean where both components are present.

6.08.3 THE NATURE OF OCEANIC MIXING

Think of the ocean in its true geometry: the ratio of its vertical to horizontal dimensions is comparable to the page of paper on which you read these words. The truly remarkable aspect of ocean mixing is that water masses can travel horizontally for tens of thousands of kilometers before being mixed away through a vertical distance of only a kilometer or so. Because the ocean is largely a stratified fluid, mixing does not occur in a spatially isotropic fashion. Fluid motion is generally suppressed by buoyancy forces in the vertical, or more properly the diapycnal direction, i.e., the direction orthogonal to the surface of constant density, so that diapycnal (approximately vertical) mixing is generally many orders of magnitude smaller than isopycnal (largely horizontal) mixing. (A more exact terminology would be "dianeutral," which is orthogonal to the local "neutral surface" (McDougall, 1987).) Despite this, each are thought to be of roughly equal importance in affecting oceanic distributions, and in fact diapycnal mixing may have a dominant impact on the behavior of large-scale ocean models (Bryan, 1987; McWilliams, 1996).

A way to compare the relative importance of diapycnal and isopycnal mixing, especially in relation to the planetary-scale circulation is to compare their effective timescales. The shorter the timescale, the greater is the influence on property distributions. The dominant timescale for global-scale ocean circulation is ~500–1,000 yr (as determined by radiocarbon measurements; see Section 6.08.6). In order to estimate the diffusive timescale, one characterizes the strength of turbulent mixing in terms of a Fickian diffusion coefficient, by analogy to molecular diffusion (see discussion in Section 6.08.3). For diapycnal mixing, the dominant length scale ranges from 300 m to 3,000 m, corresponding to a typical main thermocline thickness to nearly the entire ocean depth:

$$T_D \sim \frac{L_D^2}{\kappa_D} = \frac{10^5 - 10^7 \text{ m}^2}{10^{-5} - 10^{-4} \text{ m}^2 \text{ s}^{-1}} = 10^9 - 10^{12} \text{ s} = 30 - 30{,}000 \text{ yr} \qquad (15)$$

The actual diffusive timescale is likely in the middle of this range, since mixing appears less vigorous in the thermocline than in more weakly stratified waters (see below). For isopycnal mixing,

the dominant horizontal scales range from a few hundred kilometers to ocean basin scale (10^4 km):

$$T_I \sim \frac{L_I^2}{\kappa_I} = \frac{10^{11}-10^{14}\ \mathrm{m}^2}{10^2-10^3\ \mathrm{m}^2\ \mathrm{s}^{-1}} = 10^9-10^{12}\ \mathrm{s} = 30-30{,}000\ \mathrm{yr} \quad (16)$$

Thus, despite their large numeric disparity, their net affects are comparable, and demonstrably important with respect to the global circulation timescale. A detailed discussion of the mechanics of mixing is beyond the scope of this chapter, but it is worthwhile to outline some of their major aspects. The mechanisms of mixing differ fundamentally between the two modes, so the remaining discussion occurs in two parts: diapycnal and isopycnal mixing.

6.08.3.1 Diapycnal Mixing in the Ocean

In a stratified fluid, buoyancy resists any vertical displacement of a water parcel. For a small displacement, a fluid parcel experiences an acceleration in the opposite direction linearly dependent on the displacement l:

$$B = -\frac{g}{\rho}\frac{\partial \rho}{\partial z} l \quad (17)$$

which resembles a spring constant in a simple harmonic oscillator, whose fundamental frequency is given by

$$N = \left(-\frac{g}{\rho}\frac{\partial \rho}{\partial z} \right)^{1/2} \quad (18)$$

where ρ is the fluid density and g is the gravitational acceleration. This is often referred to as the "buoyancy frequency." If one compares the work needed to overcome the stability gradient to the energy available to turbulence from the vertical shear in the horizontal velocity field, $\partial u/\partial z$, one obtains the gradient Richardson number

$$Ri = \frac{N^2}{(\partial u/\partial z)^2} \quad (19)$$

which is a dimensionless number that is inversely related to the potential for mixing. Laboratory experiments, field observations, and numerical experimentation suggest that when Ri is sufficiently small ($\sim$0.25), vertical mixing readily occurs.

Thus, one would expect in general that diapycnal or vertical mixing would on average be suppressed by stratification. It has been suggested, partly from quasi-theoretical arguments (Gargett and Holloway, 1984), and partly on the basis of observational evidence (Gargett, 1984; Quay *et al.*, 1980; Sarmiento *et al.*, 1976), that there is an inverse relationship between N and diapycnal mixing rates generally with

$$\kappa_D \propto N^{-a} \quad (20)$$

where $1 \le a \le 2$. These suppositions are likely correct, but there probably also exists several other contributing factors that may be independent of stratification (see Gargett, 1984; Garrett, 1979).

Diapycnal mixing occurs in a number of ways within the ocean. The mechanisms include (in no particular order):

- breaking inertial and internal waves (due to the superposition of waves with different frequencies);
- shear instability (when Ri becomes small, particularly in strong currents);
- double diffusion (salt fingering caused by the difference in molecular diffusivities of heat and salt);
- tidal mixing (caused by the interaction of tidal motion with the bottom or sides; important in certain geographic areas, such as over rough terrain);
- cabbeling (due to the nonlinearity of the seawater equation of state); and
- convection (when buoyancy is decreased at the ocean surface by cooling).

Measurement of temperature variance on very small scales (often referred to as microstructure) has been used to quantify the amount of mixing that is occurring by assuming a balance between its creation by turbulence and destruction by mixing (e.g., see Kunze and Sanford, 1996; Polzin *et al.*, 1995). Such measurements typically give small mixing rates ($\sim 10^{-5}\ \mathrm{m}^2\ \mathrm{s}^{-1}$) in the open ocean. Double diffusion becomes important when warm salty water overlies cold fresher water, and results in characteristic temperature–salinity structures, and the so-called "density ratio" signatures (e.g., see Schmitt, 1990, 1994, 1998). This form of mixing counterintuitively results in an enhanced transport of more slowly (molecularly) diffusing salt over temperature, and appears to set the shape of the T–S relationship for the main thermocline water masses in the subtropical North Atlantic (Schmitt, 1981).

Overall, diapycnal mixing appears to be small in the ocean interior, i.e., $\sim 10^{-5}\ \mathrm{m}^2\ \mathrm{s}^{-1}$ (Kunze and Sanford, 1996; Ledwell *et al.*, 1993) but dramatically larger over rough topography being $\sim 10^{-4}\ \mathrm{m}^2\ \mathrm{s}^{-1}$ (Ledwell *et al.*, 2000; Polzin *et al.*, 1997) and is even larger near the ocean surface (due to wind induced mixing) and the bottom boundary layer (due to friction).

6.08.3.2 Isopycnal Mixing in the Ocean

Lateral mixing may be regarded as the result of two processes (Eckart, 1948; Garrett, 1983), stirring, which streaks out properties, thereby

sharpening gradients, and mixing, which operates on these enhanced gradients (in a "diffusive" manner) thereby homogenizing properties on smaller scales. It should be noted that lateral turbulent mixing exhibits a space-scale dependence, with κ increasing with length scale. A simple theory predicts that κ varies as $L^{4/3}$, where L is the scale of the dye patch (Stommel, 1949) although some later work indicates a somewhat weaker dependence approximating $L^{1.1}$ (Okubo, 1971). Part of the challenge is the precise definition of L in the determination. Figure 3 is an illustrative plot of some horizontal mixing estimates, showing the general scale length dependence.

This "non-Fickian behavior" arises from the fact that the range of fluid motions responsible for dispersion of a tracer depends on the size of the tracer patch in relation to the spectrum of fluid motions occurring, and the distinction between stirring and mixing (e.g., see Csanady, 1972; Rhines and Young, 1983; Young *et al*., 1982).

Mixing on the meter (subkilometer) scale is dominated by stirring due to shear dispersion by internal and inertial waves and subsequent diapycnal mixing (Young *et al*., 1982), which gives

$$\kappa_{\mathrm{IS}} \simeq \left(\frac{N}{f}\right)^2 \kappa_{\mathrm{D}} \qquad (21)$$

where the subscripts I, S, and D correspond to "isopycnal," "small scale," and "diapycnal," respectively. Here N and f are the buoyancy and the Coriolis frequencies respectively. Under typical subtropical, mid-thermocline conditions (i.e., at a few hundred meters depth at mid-latitudes), this leads to mixing rates of $\sim 0.1\ \mathrm{m^2\ s^{-1}}$ (Ledwell *et al*., 1998; Sundermeyer and Price, 1998).

At 1–30 km scales, properties begin to feel the straining effect of mesoscale eddies, which tease out properties into long streaks. The r.m.s. tracer displacement grows exponentially with time, largely due to rapid stretching of tracer along mesoscale eddy streamlines, and cross-streak mixing, both by the small scale mixing described above, and possibly vortical motions (Ledwell *et al*., 1998; Polzin *et al*., 1995). Isopycnal diffusivity on this scale approaches a few $\mathrm{m^2\ s^{-1}}$.

For space scales exceeding a hundred kilometers, mesoscale eddies prove effective in transporting, stirring and mixing tracer. Traditionally, such mixing rates are estimated from the large-scale distributions of tracers, yielding isopycnal diffusivities of order $100–1{,}000\ \mathrm{m^2\ s^{-1}}$ (e.g., see Armi and Stommel, 1983; Arons and Stommel, 1967; Jenkins, 1987, 1991, 1998; Ledwell *et al*., 1998; Olbers *et al*., 1985).

6.08.4 THEORETICAL FRAMEWORK 2: TRACER AGES

In some instances, it is possible to use specific tracer concentrations, in particular radioactive or transient tracers to define a "tracer age." The underlying premise is that the tracer age is set to zero at some starting point (usually the ocean surface) and progressively increases after contact

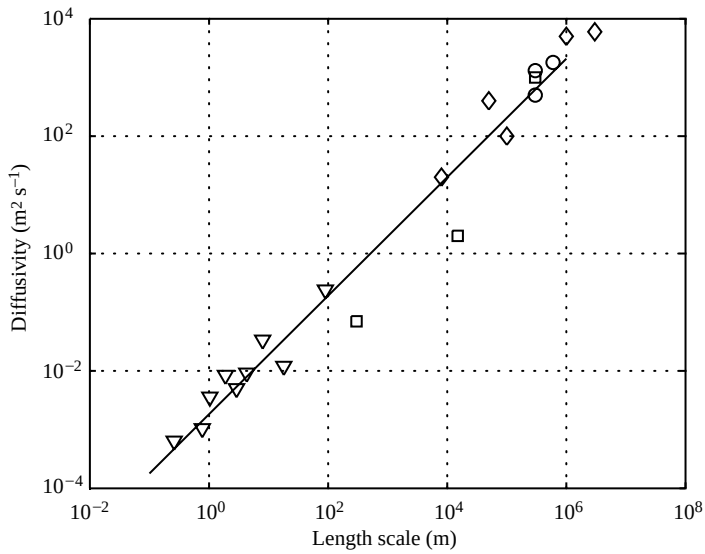

Figure 3 Some horizontal mixing estimates as a function of space scale. Results are from a small-scale float deployment (triangles, Stommel, 1949), the tracer release experiment (squares, Ledwell *et al*., 1998), and some larger-scale advection–diffusion balances (circles, see later sections) and estimates from radium isotopes (diamonds, see Section 6.08.6). The solid line represents $\kappa \propto L^1$.

is lost with its starting point. This is an attractive approach in that it provides a "direct" visualization of the pathways of ventilation and circulation. Although a useful concept in a qualitative sense, this approach is not without its complexity.

We begin by developing the concept of an ideal ventilation age (after England, 1995a; Theile and Sarmiento, 1990)

$$\frac{\partial A}{\partial t} = \kappa \nabla^2 A - \vec{u} \cdot \nabla A + 1 \qquad (22)$$

If the age A of an individual water parcel is in steady state (i.e., $\partial A/\partial t = 0$), then the age tendency term (the last term in Equation (22), the tendency to increase at a rate of 1 s s^{-1} or 1 yr yr^{-1}), is balanced by advection and diffusion of age. Such an age is different from a truly Lagrangian parcel age, which in steady state would be in the absence of mixing:

$$\vec{u} \cdot \nabla A_L = 1 \qquad (23)$$

In this case, the velocity field would seem to be obtainable directly from observation of the gradient of A_L but this is not entirely the case.

It is instructive to consider how a "real" tracer age may differ from the idealized behavior evinced by Equation (22). There are three basic tracer age techniques that have been used extensively in the literature: "radiometric dating," "transient concentration dating," and "transient concentration ratio dating." We analyze the first two approaches here. The third is too complicated to yield useful insight from simple analysis. The common thread of this discussion is that tracer ages do not necessarily represent the true ventilation age, as given by Equation (22), and in general, because of their "nonlinear" behavior, tend to *underestimate* the true age of the water (Deleersnijder *et al.*, 2001; Delhez *et al.*, 2003). Thus considerable caution should be used when interpreting such age distributions.

6.08.4.1 Radiometric Dating

Consider the transient tracer pair tritium (^{3}H) and ^{3}He:

$$^3\mathrm{H} \xrightarrow{12.5\ \mathrm{yr}} {}^3\mathrm{He} \qquad (24)$$

where tritium decays to ^{3}He with a half-life of 12.45 yr (Unterweger *et al.*, 1980). In a geochemical sense, these may be regarded as ideal tracers, since tritium, being an isotope of hydrogen, exists virtually solely as part of the water molecule, and ^{3}He is a stable, inert gas. The concept model is simple: a water parcel near the ocean surface containing tritium will not accrue any excess ^{3}He since this gas will be lost to the atmosphere. (There is, in fact, a background of atmospheric helium, containing both ^{3}He and ^{4}He. For simplicity, we will assume perfect equilibrium with the atmosphere, and will deal only with *excess* ^{3}He, ignoring the atmospheric background. Further, we will simply refer to the *excess* ^{3}He as simply "^{3}He.") Once the parcel sinks below the surface, ^{3}He begins to accumulate, and at some arbitrary time after subduction, we can compute the age of the water using

$$\tau = \frac{1}{\lambda} \ln\left(\frac{[^3\mathrm{H}] + [^3\mathrm{He}]}{[^3\mathrm{H}]} \right) \qquad (25)$$

where τ is the age, λ is the radioactive decay constant (in inverse time units), and the square brackets indicate concentration of the substances in appropriate units. The above equation can be derived in a straightforward way from the radioactive decay equation.

It is therefore possible to construct maps of this age property in the oceans, and gain an immediate qualitative grasp of the ventilation pathways and "stagnation points" in the circulation. Figure 4 is an example of this, taken from the WOCE Pacific expeditions during the early to mid-1990s. One sees the equatorward penetration of newly ventilated waters into the gyres, and the pool of old water emanating from the eastern tropics. A strong temptation arises to relate the observed age gradients to the flow field in a quantitative manner. The difficulty with this simple view arises when mixing occurs.

It is evident from inspection of Equation (25) that the mixing of water parcels with differing tritium concentrations will yield a disproportionate weighting toward the water with higher tritium. This can be quantified by considering the coupled tritium and ^{3}He advection–diffusion equations:

$$\frac{\partial \vartheta}{\partial t} = \kappa \nabla^2 \vartheta - \vec{u} \cdot \nabla \vartheta - \lambda \vartheta \qquad (26)$$

and

$$\frac{\partial \varphi}{\partial t} = \kappa \nabla^2 \varphi - \vec{u} \cdot \nabla \varphi + \lambda \vartheta \qquad (27)$$

where ϑ and φ are the tritium and ^{3}He concentrations, respectively, and both tracers are transient (see Section 6.08.7). Note the coupling imposed by the last term in each equation.

Scale analysis of the above equations reveals an interesting formulation of the Peclet number (a measure of the relative importance of advection and mixing) giving

$$Pe_R = \frac{U^2}{\kappa \lambda} \qquad (28)$$

(see Jenkins, 1988) where the subscript R distinguishes this from the traditional definition. Here the intrinsic scale length L is determined by

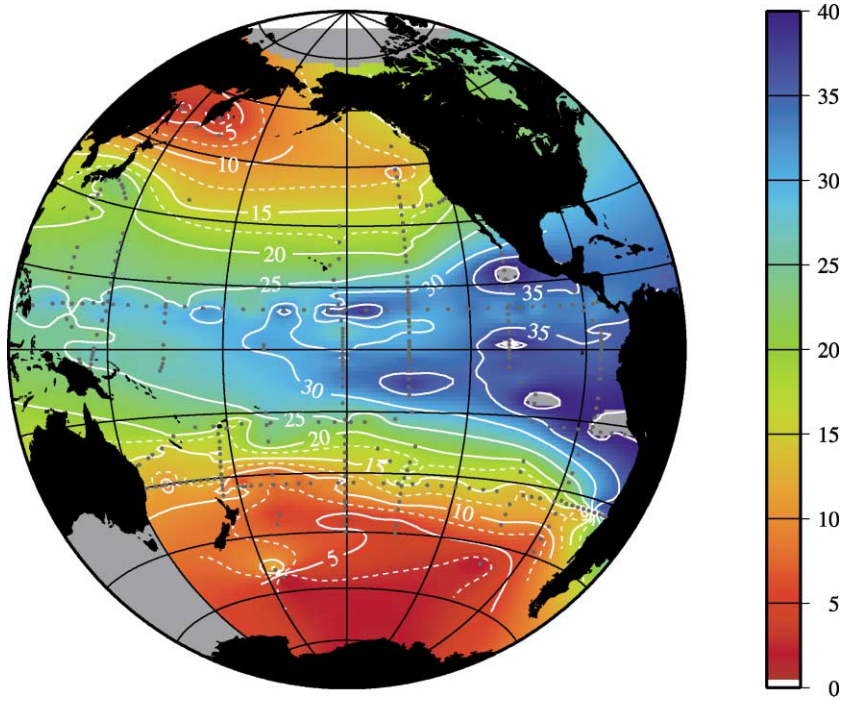

Figure 4 The distribution of tritium–^{3}He age on the $\sigma_0 = 26.5$ kg m^{-3} isopycnal during the 1990s.

the advective length over which the radiotracer decays. Consider the relationship between tritium and ^{3}He in the subtropical North Atlantic (Figure 5). The data fall in a hook-shaped pattern, corresponding to the transition between young, high tritium, low ^{3}He waters and old low tritium waters. The shape of this distribution is most comparable to a low Peclet number (~1 or less) flow in a one-dimensional stream tube simulation.

This result seems at first counterintuitive, since an estimate of the traditional Peclet number can be constructed for horizontal flow using "reasonable" mid-gyre numbers:

$$Pe = \frac{UL}{\kappa} \approx \frac{0.01\,\mathrm{m\,s^{-1}} \times 3{,}000\,\mathrm{km}}{1{,}000\,\mathrm{m^2\,s^{-1}}} = 30 \qquad (29)$$

where we have used typical large-scale isopycnal mixing rates, a typical mid-gyre velocity, and the characteristic gyre scale. The reason for the disparity can be seen by comparing the radiotracer length scale

$$L_R = \frac{U}{\lambda} \approx \frac{0.01\,\mathrm{m\,s^{-1}}}{1.7 \times 10^{-9}\,\mathrm{s^{-1}}} \approx 6{,}000\ \mathrm{km} \qquad (30)$$

That is, the radiotracer length scale exceeds the gyre scale, which means that the putative stream tube folds back on itself within the gyre circulation, short-circuiting the advective–diffusive balance, and lowering the effective Peclet number of the flow.

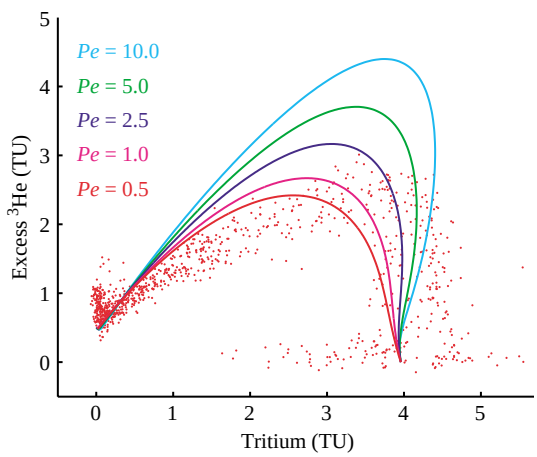

Figure 5 The tritium–^{3}He relationship for the subtropical North Atlantic in the early 1980s (solid dots). The different colored lines correspond to stream tube simulations with various values of Pe_R.

Continuing with the derivation, the two tracers may be combined by addition to provide a stable, conservative dye-tracer:

$$\zeta = \vartheta + \varphi, \qquad \frac{\partial \zeta}{\partial t} = \kappa \nabla^2 \zeta - \vec{u} \cdot \nabla \zeta \qquad (31)$$

This is a useful way of combining two coupled tracers, both of which respond to mixing and decay in a specific way, to fabricate two new composite tracers, one which responds predominantly

to decay and hence is a time tracer (the age tracer τ), and a dye tracer ζ that responds largely to dilution.

Combining the above Equations (25)–(27), and (31) with some algebraic manipulation (Jenkins, 1987, 1998), one can derive an advection–diffusion equation for the tritium–^{3}He age as

$$\frac{\partial \tau}{\partial t} = \kappa \nabla^2 \tau - \vec{u} \cdot \nabla \tau + 1 + \kappa \left(\frac{\nabla \zeta}{\zeta} + \frac{\nabla \vartheta}{\vartheta} \right) \cdot \nabla \tau \quad (32)$$

or, alternatively,

$$\frac{\partial \tau}{\partial t} = \kappa \nabla^2 \tau - \vec{u} \cdot \nabla \tau + 1 + \kappa [\nabla \ln(\zeta \vartheta)] \cdot \nabla \tau \quad (33)$$

which resembles Equation (22), except for the peculiar mixing term on the far right-hand-side. Inasmuch as it operates on the age gradient, the term appears as a pseudo-advective divergence term, and is generally negative. Consider the early days of the bomb tritium transient, when tritium was advecting and mixing into an essentially tritium-free ocean. Downstream gradients in tritium (specifically ζ and tritium) will be *negative*, which will make the mixing term the same sign as, and hence augmenting the advective term. This means that the age "signal" will propagate more rapidly into the interior, resulting in a tracer age "depression" relative to the ideal ventilation age. This is consistent with the intuitive argument made earlier about the age mixing nonlinearly because mixtures tend to favor the higher tritium end-member.

Although complicated, this relationship quantifies the effect of mixing, and can be used to assess mixing rates within the ocean (see Section 6.08.8, and Jenkins, 1998; Robbins and Jenkins, 1998; Robbins *et al*., 2000).

6.08.4.2 Transient Concentration Dating

Where atmospheric concentrations have been changing with time (e.g., as in the case of anthropogenicaly released gases), it could be argued that in the absence of mixing, water parcels could be "time stamped" with equilibrium concentrations. Thus, a fluid parcel could be assigned a vintage "V" by using the time-dependent concentration history

$$C = f(V) \quad (34)$$

providing that there is a unique (or determinable) relationship such as a monotonically increasing atmospheric abundance due to anthropogenic release. An example would be CFC-12 concentrations in the atmosphere prior to the Montreal Protocol.

Such temporal signatures would only be preserved in the absence of mixing, for dilution of recently ventilated waters with tracer-free or differently aged waters would alter the concentration and hence the inferred age in a nonlinear fashion. That is, the age of the mixture would not be equal to the mixture of the ages of the component parts. Following the work of Doney *et al*. (1997) and ignoring the second-order effects associated with the nonlinearity of the solubility function for the gas, one can derive a relationship for the age equivalent to Equation (32) by substituting (34) into (11) and expanding the derivatives using

$$\begin{aligned} \frac{\partial C}{\partial t} &= \frac{\partial f}{\partial V} \frac{\partial V}{\partial t} \\ \nabla C &= \frac{\partial f}{\partial V} \nabla V \\ \nabla^2 C &= \frac{\partial f}{\partial V} \nabla^2 V + \frac{\partial^2 f}{\partial V^2} (\nabla V)^2 \end{aligned} \quad (35)$$

and using $f' = \partial f / \partial V$, $f'' = \partial^2 f / \partial V^2$, and $\tau_C = t - V$ to obtain

$$\frac{\partial \tau_C}{\partial t} = \kappa \nabla^2 \tau_C - \vec{u} \cdot \nabla \tau_C + 1 - \kappa \left(\frac{f''}{f'} \nabla \tau_C \right) \cdot \nabla \tau_C$$

or (36)

$$\frac{\partial \tau_C}{\partial t} = \kappa \nabla^2 \tau_C - \vec{u} \cdot \nabla \tau_C + 1 + \kappa \left(\frac{f''}{(f')^2} \nabla C \right) \cdot \nabla \tau_C$$

The relationship thus derived is similar to that for the radiometric age Equation (33), with an additional pseudo-advective term related to the intensity of mixing and material gradients. An important corollary, however, is that the effect of mixing is related to the curvature of the time history of the atmospheric concentration (see Doney *et al*., 1997). Thus, if the growth rate of atmospheric concentrations were perfectly linear, we would have $f'' = 0$, so that the additional mixing term becomes zero and the age tracer obeys the ideal transient tracer age relationship:

$$\frac{\partial \tau_C}{\partial t} = \kappa \nabla^2 \tau_C - \vec{u} \cdot \nabla \tau_C + 1 \quad (37)$$

Examination of the atmospheric concentration histories for CFCs, it would appear that this would be a reasonable approximation for CFC-11 in the 1970s through early 1980s, and for CFC-12 for the 1980s, but the abrupt turnover in release curves in the early 1990s would lead to significant departures from the ideal. Further analysis of (36), however, might prove useful in studying CFC age distributions and analyzing model simulation results.

6.08.5 THEORETICAL FRAMEWORK 3: OPTIMUM MULTIPARAMETER ANALYSIS AND TRACER AGE SPECTRA

It can be argued that the concentration of a conservative, steady-state tracer C at a particular location in the ocean arises from the mixture of a number of water masses with their own characteristic concentrations C_j, which in turn were set at their "origins" (usually, but not exclusively thought of as the sea surface in a specific geographic region). In principle, if enough tracers are measured at this given location, and if the tracers are "independent," i.e., they have different water mass concentration "fingerprints," it should be possible to estimate the relative contributions of the various source water masses to the mixture. Hence for a mixture of N water masses with M distinct tracers, one has

$$\begin{aligned} X_1C_{11} + X_2C_{12} + X_3C_{13} + \cdots + X_NC_{1N} &= C_1 \\ X_1C_{21} + X_2C_{22} + X_3C_{23} + \cdots + X_NC_{2N} &= C_2 \\ &\vdots \\ X_1C_{M1} + X_2C_{M2} + X_3C_{M3} + \cdots + X_NC_{MN} &= C_M \end{aligned} \tag{38a}$$

and

$$X_1 + X_2 + X_3 + \cdots + X_N = 1 \tag{38b}$$

and for all

$$0 \le X_i \le 1 \tag{38c}$$

where C_{ij} is the ith tracer concentration of the jth source water mass, C_i is the ith tracer concentration of the resultant mixture, and X_j is the fractional contribution of the jth source water mass. Implicit within this formulation is that the properties mix conservatively (i.e., linearly). Equations (38) are a $(M+1)$ set of linear simultaneous equations in N unknowns that can be written as a matrix equation

$$S\chi = c \tag{39}$$

where χ is the vector of water mass fractions

$$\chi = \begin{bmatrix} X_1 \\ X_2 \\ \vdots \\ X_N \end{bmatrix} \tag{40}$$

c is the vector of tracer concentrations at the location in question,

$$c = \begin{bmatrix} C_1 \\ C_2 \\ \vdots \\ C_M \\ 1 \end{bmatrix} \tag{41}$$

and S is the water mass source values

$$S = \begin{bmatrix} C_{11} & C_{12} & \cdots & C_{1N} \\ C_{21} & C_{22} & \cdots & C_{2N} \\ \vdots & \vdots & \vdots & \vdots \\ C_{M1} & C_{M2} & \cdots & C_{MN} \\ 1 & 1 & \cdots & 1 \end{bmatrix} \tag{42}$$

which can be solved in a non-negative weighted least-squares sense (e.g., see Mackas *et al.*, 1987) provided that $M > N$. This achieved by minimization of the quantity

$$D^2 = (S\chi - c)^{\mathrm{T}} W^{-1} (S\chi - c) \tag{43}$$

where W is the covariance matrix for the tracers. Two important issues in this calculation are

- The choice of appropriate tracers for this constraint. The tracers must be conserved in mixing, and they should be linearly independent (i.e., they should provide unique information).
- The tracer concentrations should be normalized (i.e., weighted) to account for their relative measurement uncertainties. This is included in W.

From this, maps of the relative contribution of water masses can be made. For further discussion on the finer points of this approach, the reader is referred to numerous works by Tomczak and co-workers (e.g., Hamann and Swift, 1991; Poole and Tomczak, 1999; Tomczak, 1999; Tomczak and Large, 1989).

The approach described above is usually applied to a modest number of source water masses, typically 3–6, a number practically limited by the number of independent conservative tracers available to constrain the mixture. With a subtle shift of emphasis, it is possible to conceptually extend this approach to a continuum. Rewriting Equation (11) slightly,

$$\frac{\partial C(\vec{x},t)}{\partial t} - \kappa\nabla^2 C(\vec{x},t) + \vec{u}\cdot\nabla C(\vec{x},t) = J(\vec{x},t) \tag{44}$$

where we have made explicit the space and time dependence of both the concentration and the source/sink terms, we can then seek a Green

function solution where

$$\frac{\partial G}{\partial t} - \kappa\nabla^2 G + \vec{u}\cdot\nabla G = \delta(\vec{x}-\vec{x}')\delta(t-t') \quad (45)$$

(the right-hand side is the Dirac-delta function, or an impulse), which allows us to construct the tracer concentration at a given place and time as a superposition by the convolution

$$C(\vec{x},t) = \int \mathrm{d}^3\vec{x}' \int_{t_0}^{t} \mathrm{d}t'\, J(\vec{x}',t) G(\vec{x},t|\vec{x}',t') \quad (46)$$

That is, the Green function is a solution of the time-dependent advection–diffusion equation for a point source impulse at a location $\vec{x}'$ and time t' which has unit area:

$$\int \mathrm{d}^3\vec{x}' \int_{t_0}^{t} \mathrm{d}t'\, G(\vec{x},t|\vec{x}',t') = 1 \quad (47)$$

and hence represents a normalized weighting function for the contribution of water masses at all points in space and time to the observation point $\vec{x}$. Note that it is dependent only on the fluid flow field, and not on specific tracers: it is *tracer independent*. In a crude way of thinking, the Green function plays the role of the χ vector in Equation (39). Although it is not possible to uniquely define the structure of G over all space and time with available tracer measurements (the problem becomes underdetermined given a finite number of tracer constraints), one may seek to use tracer observations to learn about some *aspect* of the space and time structure of G.

Tracer age spectrum analysis is an important extension of this technique. (We have closely followed the discussion of Haine and Hall (2002) with a change in nomenclature to fit with usage within this chapter.) It is predicated on the recognition that a given fluid parcel represents a mixture of fluid "particles" that originated from a variety of locations at the sea surface (where the age was zero) with different transit times to reach this location. Hence, there must exist an "age spectrum" that is solely a characteristic of the fluid advective–diffusive regime. Individual tracer age measurements may represent some aspect of this age spectrum, but precisely what aspect depends on the nature of the age tracer, its history, and its boundary conditions. For a tracer with no internal sources or sinks, but which is set to some value at the ocean surface, here designated by Ω, one can construct a Green function type solution that satisfies

$$\frac{\partial G_\Omega}{\partial t} - \kappa\nabla^2 G_\Omega + \vec{u}\cdot\nabla G_\Omega = \delta(\vec{x}-\vec{x}')\delta(t-t')$$
$$\int \mathrm{d}^3\vec{x} \int_{t_0}^{t} \mathrm{d}t'\, G_\Omega(\vec{x},t|\vec{x}',t') = 1 \quad (48)$$
$$\vec{x}' \in \Omega$$

Here, G_Ω may be called the "multiple source boundary propagator," which describes the water mixture at a location along with the origin/transit times $\tau = (t-t')$ of those water masses at the sea surface. It is, by definition, dependent solely on fluid transport properties, and independent of the particular tracer. Since there are no internal sinks or sources of C, we can construct the tracer distribution in a fashion analogous to (46) with

$$C(\vec{x},t) = \int_\Omega \mathrm{d}^2\vec{x}' \int_{t_0}^{t} \mathrm{d}t' C(\vec{x}',t')\, G_\Omega(\vec{x},t|\vec{x}',t')$$
$$\vec{x}' \in \Omega \quad (49)$$

where $C(\vec{x}',t)$ gives the variation in time and space of the tracer concentration at the sea surface as a function of space and time. The attractive feature of this formulation is that it separates the dependence of the tracer distribution into the fluid transport G and the boundary condition $C(\Omega,t)$.

This approach can be connected with the tracer-age concept in the following manner. Consider the transient concentration ("vintage age") approach used for CFC distributions (see previous section). We define the tracer concentration age as

$$\tau_C(\vec{x},t) = t - V(C(\vec{x},t)) \quad (50)$$

where V is the vintage age as a function of surface concentration (i.e., the inverse of the surface concentration *versus* age function). Following the concept above we have

$$\tau_C(\vec{x},t) = t - V\left(\int_\Omega \mathrm{d}^2\vec{x}' \int_{-\infty}^{t} \mathrm{d}t' C(\vec{x}',t') \times G_\Omega(\vec{x},t|\vec{x}',t') \right) \quad (51)$$

In the special case where the surface concentration is a linear function of time (i.e., monotonically increasing), then we have $C(\Omega,t) \propto t$, so the above reduces to

$$\tau_C(\vec{x},t) = \int_\Omega \mathrm{d}^2\vec{x}' \int_0^\infty \mathrm{d}\tau\, \tau G_\Omega(\vec{x},t|\vec{x}',t-\tau)$$
$$= \int_\Omega \mathrm{d}^2 x\, A(\vec{x},t) \quad (52)$$

where A is a solution of the equation

$$\frac{\partial A}{\partial t} - \kappa\nabla^2 A + \vec{u}\cdot\nabla A = 1 \quad (53)$$

That is, the tracer concentration age of a transient tracer whose concentration in the ocean surface water is increasing in an exactly linear fashion is equal to the first moment of the age spectrum, and thus equates to an ideal age tracer. This is precisely the conclusion reached in Section 6.08.4 (Equations (36) and (37)).

This new approach is currently receiving considerable attention in oceanography, and is a useful adjunct to the traditional strategies for analysis of tracer distributions and numerical models. A number of illustrative examples have been discussed in the literature (Deleersnijder *et al.*, 2001, 2002; Delhez *et al.*, 2003; Haine and Hall, 2002; Hall and Haine, 2002).

6.08.6 STEADY-STATE TRACERS

The distributions of steady-state tracers have traditionally been used to infer the qualitative nature of ocean circulation, tracing the origins and pathways of water masses. There is a rich history that need not be repeated here. In this discussion, the distributions of dissolved oxygen and major inorganic nutrients (nitrate, phosphate, and silicate) are not utilized. The reasoning is that although they boast a long history and large database, their involvement in the carbon system and biogeochemical processes makes them suspect in drawing inferences about physical quantities. The one exception to this is the use of quasi-conservative constructs that utilize the Redfield stoichiometry to "see through" the biogeochemical "interference" in order to reconstruct water-mass histories or origins (e.g., see the discussion of optimum multiparameter analysis in the previous section) (Broecker and Peng, 1982; Broecker *et al.*, 1976, 1980b).

6.08.6.1 Radiocarbon

Despite its nonconservative behavior, however, it is important to consider radiocarbon amongst the number of examples whereby inferences have been made regarding the magnitude of mixing in the ocean using radioactive steady-state tracers. Munk (1966) and later Craig (1969) made a simple scaling calculation to estimate the net vertical mixing rate for deep Pacific by assuming that the vertical distributions of temperature and salinity were in one-dimensional advective–diffusive balance, and adding the vertical profile of natural radiocarbon to solve for mixing and vertical advection. The argument was that there existed a one-dimensional advective–diffusive subrange between the incoming common water at ~3,000 m depth and the intermediate water above at 1,000 m. They assumed that the water between these end-members was dominated by vertical mixing and advection. Here, the vertical advection is an assumed generalized upwelling of deep waters formed by sinking in polar regions. This, in turn, must be compensated by downward diffusion of heat (and other tracers) to establish steady state.

Whereas Munk ignored biogeochemical effects on the radiocarbon profiles, Craig improved the original estimate by accounting for the biological regeneration of near-surface "modern" carbon using dissolved oxygen profiles and using Redfield stoichiometry (Craig, 1969). By iteratively solving a set of simultaneous partial differential equations, they could obtain the individual mixing and advection terms. Starting with the vertical profiles of salinity and temperature (treating them as passive tracers), one has

$$\begin{aligned} \frac{\partial T}{\partial t} &= 0 = \kappa \frac{\partial^2 T}{\partial z^2} - w \frac{\partial T}{\partial z} \\ \frac{\partial S}{\partial t} &= 0 = \kappa \frac{\partial^2 S}{\partial z^2} - w \frac{\partial S}{\partial z} \end{aligned} \tag{54}$$

whose solutions are exponential curves between the end-member values which have a characteristic scale length defined by

$$z^* = \frac{\kappa}{w} \tag{55}$$

The second constraint is given by the observed oxygen profile, which satisfies

$$\frac{\partial O_2}{\partial t} = 0 = \kappa \frac{\partial^2 O_2}{\partial z^2} - w \frac{\partial O_2}{\partial z} - J_{O_2} \tag{56}$$

which provide (given z^*) an additional relationship:

$$J^* = \frac{J_{O_2}}{w} \tag{57}$$

now given a radiocarbon concentration profile, where (Note that the radiocarbon *concentration* must be used in this relationship, rather than the traditionally reported $\Delta^{14}C$, which is roughly an isotopic ratio anomaly.)

$$\frac{\partial C_{14}}{\partial t} = 0 = \kappa \frac{\partial^2 C_{14}}{\partial z^2} - w \frac{\partial C_{14}}{\partial z} - \lambda_{14} C_{14} - RJ \tag{58}$$

Here R is the known stoichiometric ratio of carbon oxygen in organic remineralization (based on observations of AOU and $\sum CO_2$ in the oceans). From the profile, one obtains

$$\lambda^* = \frac{\lambda_{14}}{w} \tag{59}$$

Since λ_{14} is a known constant, it is possible to solve Equations (55), (57), and (59) to obtain κ, w, and J. From this they obtained a net vertical mixing rate of $\sim 10^{-4}\ m^2\ s^{-1}$ which became a canonical measure of vertical mixing in the abyssal ocean.

The distribution of natural radiocarbon, with its half-life of ~5,000 yr is unique among steady-state tracers as a diagnostic of ocean mixing and circulation. Aside from its long (but not too long)

half-life, it also holds the distinction of being a very slow exchanger with the atmosphere due to the large inorganic carbonate buffer system. This latter feature will prove an interesting diagnostic of large-scale ocean models, as it is a sensitive diagnostic of the residence time of upwelled waters at the ocean surface (see Broecker and Peng, 1982; Broecker *et al.*, 1978). Moreover, this isotope is dutifully recorded in corals, providing a backwards perspective of surface ocean radiocarbon records over many centuries (e.g., Druffel, 1981). There are complications, however, to its use. First, its distribution is affected in the deep waters by remineralization of organic material raining down from above, which significantly affects its deep distributions (Craig, 1969). Second, the atmospheric inventories have been severely perturbed first by the Suess Effect (dilution with old, fossil fuel carbon (Druffel, 1981), and then subsequently by nuclear weapons produced radiocarbon (see next section). Thus, in order to effectively utilize this tracer, the different components must be sorted out (Broecker *et al.*, 1985, 1980a).

6.08.6.2 Radon-222

Within ocean sediments, the decay of uranium and thorium isotopes leads to the creation of ^{222}Rn, which is released to sedimentary pore waters and subsequently diffuses into the overlying seawater. Near the seafloor, excess ^{222}Rn can be seen against the background of a natural standing stock of this isotope in the water column, which is produced by *in situ* decay of ^{226}Ra, a long-lived and relatively uniformly distributed isotope. Because of its short half-life, the existence of this excess isotope some several hundred meters above the seafloor implies a significant flux into the bottom waters, and the shape of the profiles has been modeled as a vertical diffusive balance with radioactive decay of radon and *in situ* production from the decay of ^{226}Ra,

$$\kappa \frac{\partial^2 C_{222}}{\partial z^2} - \lambda_{222} C_{222} + \lambda_{226} C_{226} = 0 \qquad (60)$$

leading to estimates of order 10^{-4}–10^{-2} m^2 s^{-1} (Broecker *et al.*, 1968; Chung and Craig, 1972; Sarmiento and Biscaye, 1986; Sarmiento and Broecker, 1980; Sarmiento *et al.*, 1978), and have been argued to anticorrelate with the vertical stability (Sarmiento *et al.*, 1976). Although such estimates support the existence of a strong effectively vertical mixing rate near the seafloor, it is not possible to distinguish a truly local vertical mixing from shearing and advection of smaller scale bottom mixed layers from nearby topographic features (e.g., see Armi, 1977; Armi and D'Asaro, 1980; Armi and Millard, 1976).

6.08.6.3 Radium

No stable isotopes of radium exist. Radium is produced by the decay of thorium isotopes in the natural decay chain sequences, and contrary to its parent thorium, is relatively soluble and conservative in seawater. There are four isotopes, with half-lives ranging from a few days (3.7 d for ^{224}Ra, and 11.4 d for ^{223}Ra) through years (5.7 yr for ^{228}Ra) to millennia (1,600 yr for ^{226}Ra). The longest-lived isotope is relatively homogeneously distributed in the global ocean, because its decay timescale is longer than the planetary circulation timescale, but exhibits enhanced abundance near coastal regions. Moreover, the shorter-lived isotopes have the rather useful boundary condition of being dominated by production in marine sediments, particularly in continental shelf/slope environments. Here, radium levels are elevated by a combination of desorption from particles (either in river water or sediments) and direct groundwater discharge. (Radium isotopes have been used recently to quantify the magnitude of tidal groundwater pumping and direct groundwater discharge to the coastal environment, a potentially significant component for geochemical budgets of some elements for the ocean (Moore, 1997, 1999).)

Because of its short half-life, the distribution of ^{224}Ra can be sensitive indicator of small-scale horizontal mixing processes. Its distribution in Long Island Sound, a narrow embayment a few tens of kilometers wide, has been used to measure mixing rates of order 5–50 m^2 s^{-1} (Torgersen *et al.*, 1996), a value compatible with the spatial scale (see Section 6.08.3, and Ledwell *et al.*, 1998). Moore (2000) has made measurements of all four isotopes in coastal waters of the Mid-Atlantic Bight. He assumed a steady-state horizontal diffusion–decay balance:

$$\kappa \frac{\partial^2 C}{\partial x^2} = \lambda C \qquad (61)$$

where x is the off-shore distance, to compute mixing coefficients in the range 300–400 m^2 s^{-1} within 50 km of shore. Sarmiento *et al.*, 1982) modeled the distribution of ^{228}Ra on isopycnal surfaces in the North Atlantic assuming diffusion–decay balance, and estimated basin-scale horizontal mixing rates of ~6,000 m^2 s^{-1}. Huh and Ku (1998) have similarly modeled the zonal distribution of ^{228}Ra and ^{226}Ra in the northeast Pacific, yielding $\kappa \sim 100$ m^{2}s^{-1} within ~100 km of the coast, but substantially larger κ (~5,000 m^2 s^{-1}) up to 1,000 km off-shore. This latter value appears somewhat larger than conventional estimates on these space scales (e.g., see Jenkins, 1991, 1998; Ledwell *et al.*, 1998; Robbins *et al.*, 2000), and is likely a reflection of the author's choice of the simple diffusion–decay model to

model the radium distributions, ignoring the role of gyre-scale circulation and advection.

6.08.6.4 Argon-39

This extremely rare isotope of argon is produced by cosmic ray interactions in the atmosphere, and decays with a half-life of 269 yr. It offers some intriguing advantages as a steady-state tracer, most notably the ideal length of its half-life (making it useful on decade to millennial timescales) and its biogeochemical inertness (making it conservative, and hence simple). Cosmic ray production rate of this isotope have been roughly constant (±7%) over the past 1,000 years, and its gas exchange characteristics are straightforward. The biggest problem with this tracer is the challenge of obtaining and processing large seawater samples (~1 m^3 water is required per sample) and the extreme difficulty making the very low background radiometric measurements themselves. These challenges conspire to limit the amount of data available, but results in the deep eastern North Atlantic show consistency between radiocarbon and ^{39}Ar (Schlitzer *et al.*, 1985) estimates of deep water renewal rates, mixing and circulation in that area.

6.08.6.5 Dissolved Atmospheric Argon

Curiously, it appears that an inert, nonradioactive gas can provide a measure of vertical mixing rates in the ocean. This arises from the fact that seasonal heating in the subtropics leads to a supersaturation of this gas in the upper 50–100 m. The exhalation of this gas during summer months is incomplete, being restricted by stratification and slow mixing across the seasonal thermocline. Combining observations with an upper ocean seasonal model (the Price–Weller–Pinkel model modified for gas exchange: Musgrave *et al.*, 1988) reveals that the shallow argon evolution over summer months constrains vertical mixing rates near the sea surface (Spitzer and Jenkins, 1989). The mixing rate obtained, $\sim 10^{-4} m^2 s^{-1}$ is somewhat higher than thermocline mixing rates (e.g., see Ledwell *et al.*, 1993), but smaller than mixed layer rates.

6.08.7 TRANSIENT TRACERS

Embellishing the categorization made in Section 6.08.2, transient tracers can be defined as substances whose concentration distributions are changing on interannual timescales and in a noncyclical nature. Thus, dissolved oxygen or argon in the seasonal layer would be excluded from this discussion, despite the fact that their concentrations change with time due to seasonal forcing and the passage of events such as phytoplankton blooms or storms. I refer instead to tracers whose distributions have been affected on regional or global scales by humankind's activities.

Of the tracers discussed here, there have been three generic release styles. They are:

- *Nuclear weapons testing fallout*, which is characterized by a pulse-like injection into the atmosphere predominantly in the 1950s and 1960s, and includes the radioisotopes ^{3}H (tritium), ^{14}C (radiocarbon), ^{90}Sr, ^{129}I, ^{137}Cs, etc.
- *Industrial and domestic release* of substances associated with societal or military activities, such as fossil fuel CO_2, chlorofluorocarbons (CFCs) from a variety of sources, ^{85}Kr from nuclear fuel reprocessing.
- *Point source and episodic releases* of primarily radioisotopes from nuclear fuel reprocessing (e.g., Windscale effluent) and from accidents (e.g., the Chernobyl disaster).

Figure 6 is a schematic of the time history of representative tracers characterized by the first two types of release styles for the northern hemisphere. Three of the tracers (radiocarbon and the CFCs) are gaseous phase tracers, and are consequently relatively homogeneously distributed between the hemispheres, with the northern hemisphere leading the southern hemisphere by 1–2 yr: both CFCs and radiocarbon were released preferentially in the northern hemisphere. Radiocarbon was released from atmospheric nuclear weapons tests that were almost solely in the northern hemisphere, and CFC releases were dominated by North American, European, and Soviet production. The time lag

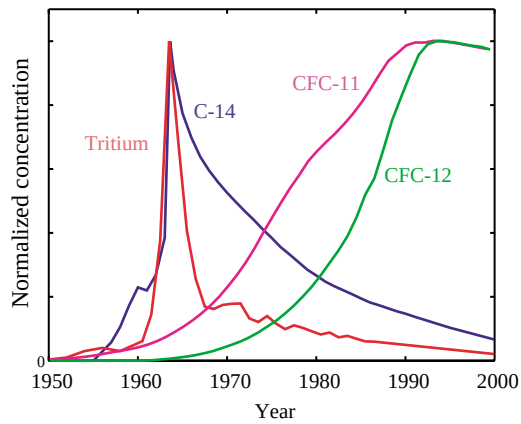

Figure 6 Normalized selected transient tracer histories for the northern hemisphere.

between northern- and southern-hemispheric abundances is characteristic of the exchange timescale between the two hemispheres in the troposphere.

Tritium, however, was largely released directly to the stratosphere, where it is oxidized to tritiated water vapor. It is subseqently mixed back into the troposphere, predominantly at mid-latitudes and rapidly rained out as tritiated rainfall (e.g., see Weiss and Roether, 1980). Thus, there is a far greater asymmetry between the two hemispheres, and characteristically different "deposition" histories. Figure 7 shows the first two EOFs of the tritium in precipitation as analyzed by Doney (Doney *et al.*, 1992) from IAEA data. The pattern decomposes into two dominant factors: a northern impulse (the largest component) and a smaller, more diffuse southern component.

Another difference arises from the way in which the tracers are introduced into the ocean. CFCs have the simplest boundary conditions, as they dissolve as inert gases, following gas exchange and solubility rules (Warner *et al.*, 1996; Warner and Weiss, 1985). A typical gas exchange timescale for CFCs is of order 1–2 months, depending on wind speed and mixed-layer depth. Radiocarbon also enters the ocean via gas exchange (as CO_2), but its gas exchange timescale is amplified by the large isotopic inertia associated with the carbonate system in seawater. Thus, the gas exchange timescale for radiocarbon is much longer, i.e., of order 10–12 yr (Broecker and Peng, 1982). Tritium, however, is deposited by both direct precipitation and water vapor exchange:

$$D_{\text{atm}} = PC_{\text{P}} + E\frac{h}{1-h}C_{\text{V}} - E\frac{1}{\alpha(1-h)}C_{\text{S}} \quad (62)$$

where P and E are the precipitation and evaporation rates, C_{P}, C_{V}, and C_{S} are the tritium concentrations in precipitation, atmospheric water vapor, and the sea surface, respectively, and where h and α are the relative humidity and isotopic fractionation factor (Weiss and Roether, 1980).

The impact of the difference in the boundary conditions between tracers can be seen in Figure 8, which compares the meridional distributions of tritium and CFC-11 in the central Pacific. The common element of both distributions is the tongue of elevated tracer concentrations being subducted in the northern subtropics, advected equatorward, and upwelled in the tropics. This feature was first noted in tritium by Fine *et al.* (1981, 1983, 1987) and places important constraints on the exchange timescales for subtropical–tropical overturning in the Pacific. This, in turn is potentially an important regulatory element

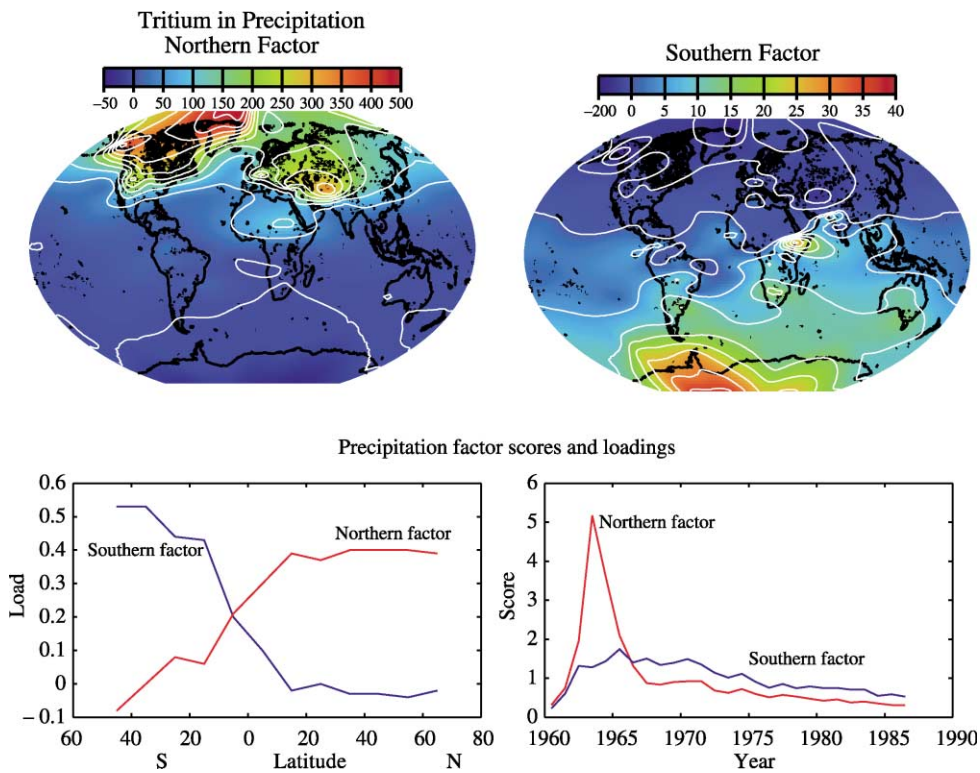

Figure 7 The northern and southern EOFs for tritium concentrations in precipitation (after Doney *et al.*, 1992).

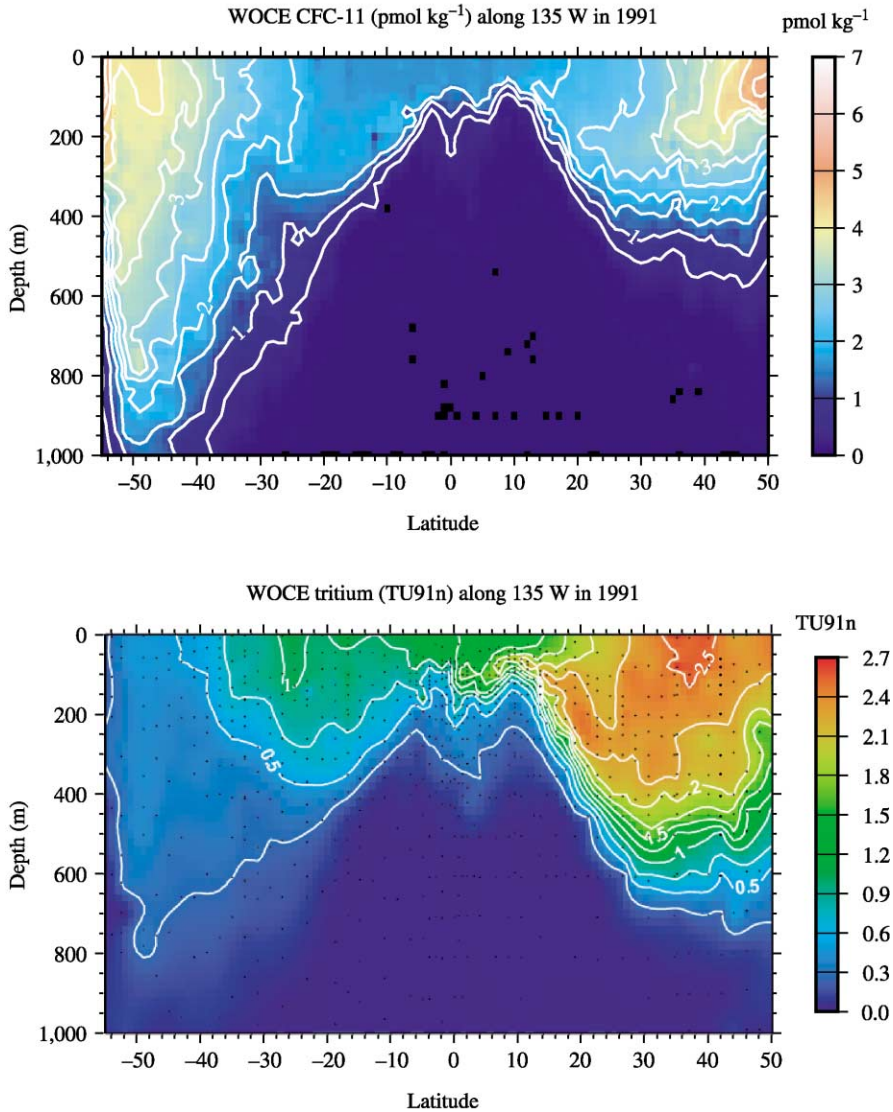

Figure 8 The meridional distributions of CFC-11 (upper panel) and tritium (lower panel) along 135° W in the Pacific during the WOCE expedition. CFC data were obtained from the WHPO data release no. 3 (see also Bullister *et al.*, 2000; Fine *et al.*, 2001; Schlosser, *et al.*, 2001).

in decadal variations in El Nino/ENSO strength (An and Jin, 2001; Deser *et al.*, 1996; Gu and Philander, 1997; Guilderson and Schrag, 1997; Zhang *et al.*, 1998).

The contrast between these tracers is rooted in the pronounced meridional asymmetry in the tritium pattern (lower-southern-hemispheric values), compared to the more balanced CFC distribution. Another aspect is the northern mid-latitude maximum in tritium compared to a poleward enhancement of CFC-11. The latter is a result of the temperature dependence of CFC solubility, but the former arises from the progressive sequestration of tritium in the subtropical gyres, a phenomenon similar to that of radiocarbon (see Broecker *et al.*, 1985), and driven by the unique temporal history and depositional mode of the tracer. Such contrasting behavior is an important attribute that can be exploited in mixing calculations and model evaluation.

Multitracer approaches offer the most powerful constraints on mixing and ventilation. For example, Schlosser and co-workers have exploited the differing time histories and boundary conditions of a suite of tracers (notably tritium, ^{3}He, CFCs, radiocarbon, and ^{39}Ar) to study Arctic ventilation and mixing (Schlosser *et al.*, 1990, 1994, 1995b), and to demonstrate climatic variations in deep water formation in the Greenland/Norwegian Seas (Schlosser *et al.*, 1991, 1995a; Schlosser and Smethie, 1995).

There are four basic, but overlapping approaches to using transient tracers. They include:

- *Flow visualization,* where the tracer is, and where it is not, what pathways does it trace on entering the ocean, and what scales of dilution are occurring.
- *Direct "age" computation*, based on simple aging or vintage models (see Sections 6.08.4 and 6.08.8). The argument is that the tracer age distribution resembles the *ideal* age distribution to some approximation.
- *Diagnostic calculations,* using observed tracer distributions (e.g., tracer or age gradients, or relationships with other tracers) it may be possible to calculate mixing, velocity or ventilation rates directly within the context of simple advective–diffusive or box models.
- *Comparison with prognostic models,* by comparing observed tracer fields with model simulations, it may be possible to improve choice of model parametrizations, identify regions or processes where the model does/does not perform well

To some extent, all of these approaches have been used with some success over recent years. In the remainder of this section, I discuss some illustrative examples, with emphasis on the third of these approaches.

There are many examples of how transient tracers have been used to visualize ventilation pathways, but perhaps the most striking are the sections across the deep western boundary current (DWBC) in the North Atlantic. An early section of tritium across the DWBC (Jenkins and Rhines, 1980) revealed a strikingly outlined high tritium core which indicated the rapid southward flow of recently ventilated water. There were a number of significant attributes of this observation, however: (i) the dislocation of the tracer maximum from the high velocity core, (ii) the scale of dilution (about 10 : 1) relative to the source waters, and (iii) the remarkable absence of Labrador Sea Water tritium. The first two features hinted at the scale of the recirculation impact on entrainment and detrainment in the DWBC and the resultant downstream tracer propagation speed (see Doney and Jenkins, 1994), and the last underlined the importance of climatic variations in Labrador Sea Water formation. This was shown clearly in subsequent DWBC transections by Smethie, Fine, and others (Fine and Molinari, 1988; Pickart *et al.*, 1989, 1996; Smethie, 1993).

The penetration of tritium into the thermocline has been used to estimate vertical and diapycnal mixing rates. The first quantitative attempt was by Rooth and Ostlund (1972), who utilized an empirical relationship between bomb-tritium and temperature in the main thermocline to construct a pair of coupled advection–diffusion equations, and use the empirical relationship to eliminate advective terms in the equations, and solve for mixing rates. Starting with the advection–diffusion equations for tritium and temperature:

$$\begin{aligned}\frac{\partial C}{\partial t} &= \kappa_\rho \nabla_\rho^2 C - \vec{u}\cdot\nabla_\rho C - \lambda C \\ 0 &= \kappa_\rho \nabla_\rho^2 T - \vec{u}\cdot\nabla_\rho T\end{aligned} \tag{63}$$

they recognized a log–log relationship between the temperature and tritium within the thermocline:

$$\phi = \mu\theta + \phi_0 \tag{64}$$

where

$$\phi = \ln C \qquad \text{and} \qquad \theta = \ln(T - 2.3) \tag{65}$$

The choice of the 2.3 °C offset in the temperature transformation was predicated on the assumption that the vertical temperature distribution was pinned at the lower end by North Atlantic Deep Water flow. Transforming and rearranging Equations (63) with the definitions in (65) gives

$$\begin{aligned}\frac{\partial \phi}{\partial t} + \vec{u}\cdot\nabla_\rho\phi + \lambda &= \kappa_\rho((\nabla_\rho\phi)^2 + \nabla_\rho\kappa\cdot\nabla_\rho\phi + \nabla_\rho^2\phi) \\ \vec{u}\cdot\nabla_\rho\theta &= \kappa_\rho((\nabla_\rho\theta)^2 + \nabla_\rho\kappa\cdot\nabla_\rho\theta + \nabla_\rho^2\theta)\end{aligned} \tag{66}$$

and coupling the equations with the empirical relationship expressed in (64), they obtained

$$\begin{aligned}\frac{\partial \phi}{\partial t} + \lambda &= \left(\mu^2 - \mu\right)\kappa_\rho(\nabla_\rho\theta)^2 \\ &\approx \left(\mu^2 - \mu\right)\left(\frac{\kappa_D}{H^2} + \frac{\kappa_I}{L^2}\right)\end{aligned} \tag{67}$$

which relates the time evolution of the tritium distribution in the main thermocline to the large scale diffusive temperature fluxes, and ultimately to the spatial scales (H for vertical or diapycnal length, and L for horizontal or isopycnal) of temperature gradients. Using the empirical slope $\mu \approx 5$ and the vertical thermal scale height for the main thermocline $H \approx 440\,\text{m}$, they obtained

$$\begin{aligned}1.8\times10^{-5} &\le \left(\kappa_D + \frac{H^2}{L^2}\kappa_I\right) \\ &\le 2.3\times10^{-5}\,\text{m}^2\,\text{s}^{-1}\end{aligned} \tag{68}$$

and argued that since the second term is positive definite, sets an upper bound on diapycnal diffusion in the thermocline of $\sim 2 \times 10^{-5}\,\text{m}^2\,\text{s}^{-1}$.

The significance of this analysis was that it was the first tracer-based estimate of diapycnal diffusivity that pointed to relatively low mixing rates in the thermocline ($2 \times 10^{-5}\,\text{m}^2\,\text{s}^{-1}$),

smaller than the canonical values derived from the earlier "abyssal recipes" papers, and much smaller than average *vertical* mixing rates estimated by simple one-dimensional calculations (e.g., see Li *et al.*, 1984). These lower values were supported by consideration of the relationship between bomb-tritium and its daughter isotope ^{3}He in the thermocline (Jenkins, 1980), by a subsequent analysis of tritium profiles in the North Pacific (Kelley and Van Scoy, 1999), and by tracer release experiments in the North Atlantic (see Section 6.08.9). Resolution of this apparent discrepancy lies in the recognition that the one-dimensional balance calculation incorporates an *effective* vertical mixing rate that is a composite between true diapycnal mixing and isopycnal mixing along sloping isopycnal surfaces. Put another way, the vertical mixing rate of Li *et al.* (Li and Garrett, 1997) is dominated by off-diagonal elements in the eddy diffusion tensor in Equation (12).

Considerable progress has been made in comparing models to tracer distributions, both for radiocarbon (Rodgers *et al.*, 1999) and for CFCs (England, 1995b; England *et al.*, 1994; England and Maier-Reimer, 2001). The ability of models to replicate tracer observations is a strong function of mixing parametrization. The success and utility of future comparisons will depend strongly on the existence of a uniformly high-quality data set of as many tracers as possible, and an improved understanding of the boundary conditions and histories of these tracers.

6.08.8 TRACER AGE DATING

Although a compelling intuitive concept for yielding insights into ocean ventilation (see Figure 4) tracer age dating is affected by the nonideal behavior in the presence of mixing. This significantly complicates interpretation(e.g., see Doney *et al.*, 1997; Robbins and Jenkins, 1998), but this complication can be mastered and exploited in a constructive way. An example of this is a study carried out in the "subduction area," a well-surveyed region in the eastern subtropical North Atlantic. The distributions of tritium and ^{3}He were determined over an ~1,500 km by 1,500 km area and analyzed on isopycnal surfaces. The approach was to combine information provided by geostrophic balance (relative to some deeper reference level) with advective–diffusive balance for tritium–helium age and salinity. The subsurface distribution of the tracers is demonstrably dominated by isoycnal processes, so the balance on a given isopycnal can be expressed as

$$\frac{\partial \tau}{\partial x}u_{\mathrm{r}} + \frac{\partial \tau}{\partial y}v_{\mathrm{r}} - (\nabla_\rho^2 \tau + \nabla \ln(\zeta\vartheta)\cdot\nabla\tau)\kappa_\rho = 1 - \frac{\partial \tau}{\partial t} - \frac{\partial \tau}{\partial x}u_{\mathrm{g}} - \frac{\partial \tau}{\partial y}v_{\mathrm{g}} \qquad (69)$$

and

$$\frac{\partial S}{\partial x}u_{\mathrm{r}} + \frac{\partial S}{\partial y}v_{\mathrm{r}} - (\nabla_\rho^2 S)\kappa_\rho = 1 - \frac{\partial S}{\partial x}u_{\mathrm{g}} - \frac{\partial S}{\partial y}v_{\mathrm{g}} \qquad (70)$$

where x and y refer to the along isopycnal east and northward directions, and the subscripts r and g refer to the reference-level and geostrophic velocity components. The terms on the right-hand side of Equations (69) and (70) are known (measured) for each surface, along with the gradients and Laplacians on the left-hand side. The unknowns are the reference level velocity components u_{r} and v_{r}, and the isopycnal diffusivity κ_ρ, the latter of which is allowed to be a function of isopycnal surface. Thus, for a selection of N isopycnal surfaces, one obtains a set of $2N$ equations with $N + 2$ unknowns (N isopycnal diffusivities, and 2 reference-level velocity components). This may be solved in a least squares sense to obtain both absolute velocities, and isopycnal mixing rates as a function of depth (see Figure 9), along with their statistical uncertainties.

Note the general structure of the isopycnal mixing rate as a function of depth: the gradual decrease into the deeper thermocline is consistent with expectations, but the lower values near the surface appear problematic. This surface decrease is likely a result of ignoring possible unsteady terms in the salinity Equation (70) on the shallowest surfaces.

An additional interpretive strategy is to analyze the temporal evolution of the tracer age field. Although the magnitude of the nonlinear terms in Equation (33) are now small (Jenkins, 1987, 1998), the early evolution of the tritium transient was characterized by large nonlinearities, so that the present age distribution is still relaxing on deeper density horizons, where adjustment times are large (Robbins and Jenkins, 1998). This can be used to advantage, as the temporal evolution, and the spatial structure of the age fields become sensitive to mixing rates and ventilation pathways. This has been used to quantify the mixing of material across the Azores front, and its role in ventilation of the deep thermocline (Robbins *et al.*, 2000).

6.08.9 TRACER RELEASE EXPERIMENTS

Dye release experiments have been performed in the marine environment for many decades, but

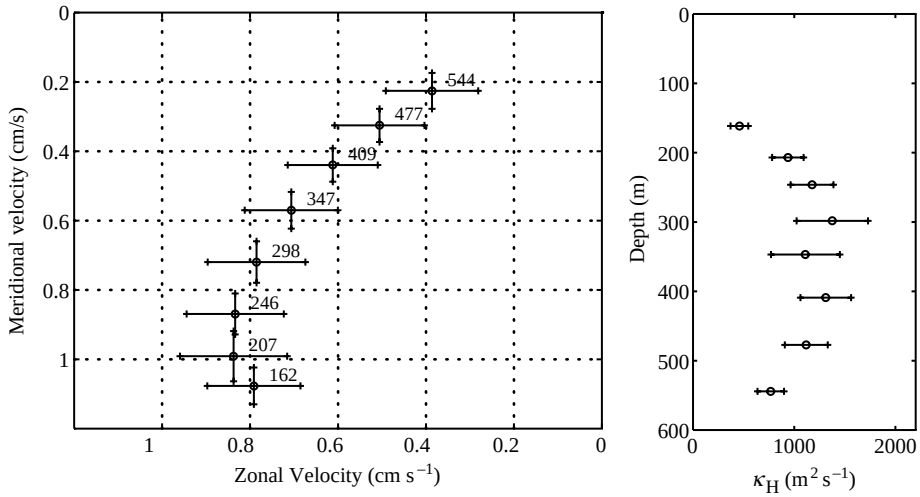

Figure 9 Tracer age estimated absolute velocities (left panel, with numbers indicating depth) and isopycnal mixing coefficients (right panel).

suffered from limitations in the scale of the release, and the complication of nonconservative behavior in some of the dyes used. However, recent technical improvements in deployment and measurement technology has resulted in a series of definitive experiments on a large enough scale to compare with traditional tracer measurements. Early experiments releasing SF_6 were performed in the Santa Monica Basin (Ledwell and Watson, 1991) which revealed a relatively weak interior diapycnal mixing rate ($\sim 2.5 \times 10^{-5}$ m^2 s^{-1}). Once the tracer had reached the basin walls, however, boundary mixing contributed to its vertical spread, leading to a substantially larger effective mixing rate (Ledwell and Bratkovich, 1995; Ledwell and Hickey, 1995).

The SF_6 release experiment was scaled up and performed at a depth of ~300 m in the North Atlantic main thermocline of the subduction area in 1992 (Ledwell *et al.*, 1993), where the dye patch was monitored for 2.5 yr. During this time, the distribution of dye in the vertical evolved as a spreading Gaussian profile, whose vertical scale increased with time consistent with a diapycnal mixing rate of initially $(1.2 \pm 0.2) \times 10^{-5}$ m^2 s^{-1} and subsequently a somewhat larger rate of $(1.7 \pm 0.2) \times 10^{-5}$ m^2 s^{-1}, confirming the earlier tracer work, and being consistent with microstructure based estimates made locally (St. Laurent and Schmitt, 1999).

Analysis of the early spread of the SF_6 dye patch on isopycnals revealed isopycnal mixing rates of order 0.07 m^2 s^{-1} for spatial scales of 100–1,000 m, which increased to 2 m^2 s^{-1} on 1–10 km scales. At this intermediate stage, the character of the tracer patch was dominated by straining and streaking by the mesoscale eddy field, and the streaks grew at an exponential rate. At the terminal stages of the experiment, mesoscale eddies dominated mixing, with effective mixing rates approaching 1,000 m^2 s^{-1} (Ledwell *et al.*, 1998), values consistent with float statistics obtained during the experiment (Sundermeyer and Price, 1998).

The presence of relatively weak diapycnal mixing below the main thermocline, however, appears problematic in terms of interpreting the large-scale one-dimensional balances studied by Munk and Craig. Turbulent dissipation measurements reveal that diapycnal mixing is weak over smooth ocean floor, but highly enhanced over rough topography (St. Laurent *et al.*, 2001; Toole *et al.*, 1994) due to tidal interaction with terrain. This was dramatically demonstrated by another tracer release experiment, this time in the abyssal Brazil Basin (Ledwell *et al.*, 2000; Polzin *et al.*, 1997) where mixing rates of $\sim(2-4) \times 10^{-4}$ m^2 s^{-1} were observed in the water column over rough topography, and values approaching 10^{-3} m^2 s^{-1} were reached near the seafloor. Such values, when regionally averaged, lead to sufficiently large mean mixing rates to close buoyancy budgets for the abyssal Brazil Basin based on large-scale hydrography (Morris *et al.*, 2001).

6.08.10 CONCLUDING REMARKS

Thinking about the use of tracers to study ocean mixing has evolved since the halcyon days of GEOSECS. The simple questions of "what is the vertical mixing rate?" and "what is the age of the deep water?" have become much more complex with the realization that the tools we are using require considerable skill and have intrinsic limitations. The oceans and the practice of oceanography have become much more complicated with time. However, the pictures of evolving

transient tracer fields that are emerging from WOCE and CLIVAR efforts are compelling and evocative. The large-scale structures are both reassuringly consistent with what we know about ocean ventilation, circulation and mixing, and yet also show a wealth of detail and structure that promises more insight into physical processes in the ocean. The challenge is utilizing this information in an effective and quantitative way.

The ocean modeling community is beginning to provide us with simulated tracer fields that are beginning to more realistically resemble the observations, but with informative differences. Modelers are increasingly turning to tracers (beyond temperature and salinity) for model evaluation, testing and validation (England and Maier-Reimer, 2001). The areas of agreement and disparity are important diagnostics of model performance and parametrization. Such tests are critical if reliable global change predictions are to be produced by such simulations. The ability of such models to "get the right answer for the wrong reasons" is a serious concern, but the risk becomes increasingly remote as additional independent tracer fields are added as constraints.

A limitation of tracer constraints on oceanic processes is the sparseness of data, and imperfectly known boundary conditions such as air–sea behavior and history. We should consider improving global coverage of tracer measurements, as well as targeted process-oriented experiments to improve on the former. We also ought to encourage activities that make inroads in the latter. The primary advantage of transient tracers lies in the time evolution of their distributions. This, coupled with the clear indication that the physical environment is changing as well, leads us to the conclusion that repeat observations are not just a luxury, but a necessity.

REFERENCES

An S.-I. and Jin F.-F. (2001) Collective role of thermocline and advective feedbacks in the ENSO mode. *J. Climatol.* **14**, 3421–3432.

Armi L. (1977) Dynamics of the bottom boundary layer of the deep ocean. In *Bottom Turbulence, Proceedings of the 8th International Liege Colloqium on Ocean Hydrodynamics* (ed. J. C. J. Nihoul). Elsevier, New York, pp. 153–164.

Armi L. (1979) The effects of variations in eddy diffusivity on property distributions in the ocean. *J. Mar. Res.* **37**, 515–530.

Armi L. and D'Asaro E. A. (1980) Flow structures of the Benthic ocean. *J. Geophys. Res.* **85**(C1), 469–484.

Armi L. and Millard R. C. (1976) The bottom boundary layer of the deep ocean. *J. Geophys. Res.* **81**(27), 4983–4990.

Armi L. and Stommel H. (1983) Four views of a portion of the North Atlantic subtropical gyre. *J. Phys. Oceanogr.* **13**, 828–857.

Arons A. B. and Stommel H. (1967) On the abyssal circulation of the world ocean: III. An advection-lateral mixing model of the distribution of a tracer property in an ocean basin. *Deep-Sea Res.* **14**, 441–457.

Broecker W. S. and Peng T. H. (1982) *Tracers in the Sea.* Eldigio Press, Palisades, NY.

Broecker W. S., Cromwell J., and Li Y.-H. (1968) Rates of vertical eddy diffusion near the ocean floor based on measurements of the distribution of excess ^{222}Rn. *Earth Planet. Sci. Lett.* **5**, 101–105.

Broecker W. S., Takahashi T., and Li Y.-H. (1976) Hydrography of the central Atlantic: I. The two-degree discontinuity. *Deep-Sea Res.* **23**, 1083–1104.

Broecker W. S., Peng T. H., and Stuiver M. (1978) An estimate of the upwelling rate in the equatorial Atlantic based on the distribution of bomb radiocarbon. *J. Geophys. Res.* **83**(C12), 6179–6186.

Broecker W. S., Peng T. H., and Takahashi T. (1980a) A strategy for the use of bomb-produced radiocarbon as a tracer for the transport of fossil fuel CO_2 into the deep-sea source regions. *Earth Planet. Sci. Lett.* **49**, 438–463.

Broecker W. S., Takahashi T., and Stuiver M. (1980b) Hydrography of the central Atlantic: II. Waters beneath the two-degree discontinuity. *Deep-Sea Res.* **27A**, 397–419.

Broecker W. S., Peng T. H., Ostlund H. G., and Stuiver M. (1985) The distribution of bomb radiocarbon in the ocean. *J. Geophys. Res.* **90**(C4), 6953–6970.

Bryan F. (1987) Parameter sensitivity of primitive equation ocean general circulation models. *J. Phys. Oceanogr.* **17**(7), 970–985.

Bullister J. L., Fine R. A., Smethie W. M., Warner M. J., and Weiss R. F. (2000) Global integration and interpretation of WOCE CFC data. *USWOCE Report* **12**, 21–25.

Chung J.-Y. and Craig H. (1972) Excess radon and temperature profiles from the eastern equatorial Pacific. *Earth Planet. Sci. Lett.* **14**, 55–64.

Craig H. (1969) Abyssal carbon and radiocarbon in the Pacific. *J. Geophys. Res.* **74**(23), 5491–5506.

Csanady G. T. (1972) *Turbulent Diffusion in the Environment.* Reidel, Boston, MA.

Deleersnijder E., Campin J.-M., and Delhez E. J. M. (2001) The concept of age in marine modelling: I. Theory and preliminary model results. *J. Mar. Syst.* **28**, 229–267.

Deleersnijder E., Mouchet A., Delhez E. J. M., and Beckers J.-M. (2002) Transient behavior of water ages in the world ocean. *Math. Comp. Model.* **36**, 121–127.

Delhez E. J. M., Deleersnijder E., Mouchet A., and Beckers J.-M. (2003) A note on the age of radioactive tracers. *J. Mar. Syst.* **38**, 277–286.

Deser C., Alexander M. A., and Timlin M. S. (1996) Upper-ocean thermal variations in the North Pacific during 1970–1991. *J. Clim.* **9**, 1840–1855.

Doney S. C. and Jenkins W. J. (1988) The effect of boundary conditions on tracer estimates of thermocline ventilation rates. *J. Mar. Res.* **46**, 947–965.

Doney S. C. and Jenkins W. J. (1994) Ventilation of the deep western boundary current and abyssal western North Atlantic: estimates from tritium and ^{3}He distributions. *J. Phys. Oceanogr.* **24**, 638–659.

Doney S. C., Glover D. M., and Jenkins W. J. (1992) A model function of the global bomb-tritium distribution in precipitation, 1960–1986. *J. Geophys. Res.* **97**, 5481–5492.

Doney S. C., Jenkins W. J., and Bullister J. L. (1997) A comparison of ocean tracer dating techniques on a meridional section in the eastern North Atlantic. *Deep-Sea Res.* **44**(4), 603–626.

Druffel E. R. M. (1981) Radiocarbon in annual coral rings from the eastern tropical Pacific Ocean. *Geophys. Res. Lett.* **8**(1), 59–61.

Eckart C. (1948) An analysis of the stirring and mixing processes in incompressible fluids. *J. Mar. Res.* **7**(3), 265–275.

England M. H. (1995a) The age of water and ventilation timescales in a global ocean model. *J. Phys. Oceanogr.* **25**(11), 2756–2777.

England M. H. (1995b) Using chlorofluorcarbons to assess ocean climate models. *Geophys. Res. Lett.* **22**(22), 3051–3054.

England M. H. and Maier-Reimer E. (2001) Using chemical tracers to assess ocean models. *Rev. Geophys.* **39**(1), 29–70.

England M. H., Garcon V., and Minster J.-F. (1994) CFC uptake in a world ocean model: 1. Sensitivity to the surface gas forcing. *J. Geophys. Res.* **99**(C12), 25215–25233.

Fine R. A. and Molinari R. L. (1988) A continuous deep western boundary current between Abaco (26.5N) and Barbados (13N). *Deep-Sea Res.* **35**(9), 1441–1450.

Fine R. A., Reid J. L., and Ostlund H. G. (1981) Circulation of tritium in the Pacific Ocean. *J. Phys. Oceanogr.* **11**, 3–14.

Fine R. A., Peterson W. H., Rooth C. G., and Ostlund H. G. (1983) Cross-equatorial tracer transport in the upper waters of the Pacific Ocean. *J. Geophys. Res.* **88**, 763–769.

Fine R. A., Peterson W. H., and Ostlund H. G. (1987) The penetration of tritium into the tropical Pacific. *J. Phys. Oceanogr.* **17**, 553–564.

Fine R. A., Maillet K. A., Sullivan K. F., and Willey D. (2001) Circulation and ventilation flux of the Pacific Ocean. *J. Geophys. Res.* **106**(C10), 22159–22178.

Gargett A. E. (1984) Vertical eddy diffusivity in the ocean interior. *J. Mar. Res.* **42**, 359–393.

Gargett A. E. and Holloway G. (1984) Dissipation and diffusion by internal wave breaking. *J. Mar. Res.* **42**(1), 15–27.

Garrett C. (1979) Mixing in the ocean interior. *Dyn. Atmos. Oceans* **3**, 239–265.

Garrett C. (1983) On the initial streakiness of a dispersing tracer in two- and three-dimensional turbulence. *Dyn. Atmos. Oceans* **7**, 265–277.

Garrett C. (1989) A mixing length interpretation of fluctuations in passive scalar concentration in homogeneous turbulence. *J. Geophys. Res.* **94**(C7), 9710–9712.

Gent P. R. and McWilliams J. C. (1990) Isopycnal mixing in ocean circulation models. *J. Phys. Oceanogr.* **20**, 150–155.

Gent P. R., Willebrand J., McDougall T. J., and McWilliams J. C. (1995) Parameterizing eddy-induced tracer transports in ocean circulation models. *J. Phys. Oceanogr.* **25**, 463–474.

Gu D. and Philander S. G. (1997) Interdecadal climate fluctuations that depend on exchanges between the tropics and extratropics. *Science* **275**, 805–807.

Guilderson T. and Schrag D. (1997) Abrupt shift in subsurface temperatures in the tropical Pacific associated with changes in El Niño. *Science* **281**, 240–243.

Haine T. W. N. and Hall T. M. (2002) A generalized transport theory: water-mass composition and age. *J. Phys. Oceanogr.* **32**, 1932–1946.

Hall T. M. and Haine T. W. N. (2002) On ocean transport diagnostics: the idealized age tracer and the age spectrum. *J. Phys. Oceanogr.* **32**(6), 1987–1991.

Hamann I. M. and Swift J. H. (1991) A consistent inventory of water mass factors in the intermediate and deep Pacific Ocean derived from conservative tracers. *Deep-Sea Res.* **38**(suppl.1), S129–S169.

Huh C.-A. and Ku T.-L. (1998) A 2-D section of ^{228}Ra and ^{226}Ra in the northeast Pacific. *Oceanolog. Acta* **21**(4), 533–542.

Jenkins W. J. (1980) Tritium and ^{3}He in the Sargasso Sea. *J. Mar. Res.* **38**, 533–569.

Jenkins W. J. (1984) The use of tracers and water masses to estimate rates of respiration. In *Heterotrophic Activity in the Sea* (eds. J. E. Hobbie and P. L. Williams). Plenum, New York, pp. 391–403.

Jenkins W. J. (1987) ^{3}H and ^{3}He in the beta triangle: observations of gyre ventilation and oxygen utilization rates. *J. Phys. Oceanogr.* **17**, 763–783.

Jenkins W. J. (1988) Using anthropogenic tritium and 3He to study subtropical gyre ventilation and circulation. *Phil. Trans. Roy. Soc. London* **A325**, 43–61.

Jenkins W. J. (1991) Determination of isopycnal diffusivity in the Sargasso Sea. *J. Phys. Oceanogr.* **21**, 1058–1061.

Jenkins W. J. (1998) Studying thermocline ventilation and circulation using tritium and ^{3}He. *J. Geophys. Res.* **103**, 15817–15831.

Jenkins W. J. and Rhines P. B. (1980) Tritium in the deep North Atlantic Ocean. *Nature* **286**, 877–880.

Jenkins W. J. and Wallace D. W. R. (1992) Tracer based inferences of new primary production in the sea. In *Primary Production and Biogeochemical Cycles in the Sea* (eds. P. G. Falkowski and A. D. Woodhead). Plenum, New York, pp. 299–316.

Joyce T. M. and Jenkins W. J. (1993) Spatial variability of subducted water in the North Atlantic. *J. Geophys. Res.* **98**, 10111–10124.

Kelley D. and Van Scoy K. A. (1999) A basin-wide estimate of vertical mixing in the upper pycnocline: spreading of bomb tritium in the North Pacific Ocean. *J. Phys. Oceanogr.* **19**, 1759–1771.

Kunze E. and Sanford T. B. (1996) Abyssal mixing: where it is not. *J. Phys. Oceanogr.* **26**(10), 2286–2296.

Ledwell J. R. and Bratkovich A. (1995) A tracer study of mixing in the Santa Cruz basin. *J. Geophys. Res.* **100**(C10), 20681–20704.

Ledwell J. R. and Hickey B. M. (1995) Evidence for enhanced boundary mixing in the Santa Monica basin. *J. Geophys. Res.* **100**(C10), 20665–20679.

Ledwell J. R. and Watson A. (1991) The Santa Monica basin tracer experiment: a study of diapycnal and isopycnal mixing. *J. Geophys. Res.* **96**(C5), 8695–8718.

Ledwell J. R., Watson A. J., and Law C. S. (1993) Evidence for slow mixing rates across the pycnocline from an open-ocean tracer-release experiment. *Nature* **364**, 701–703.

Ledwell J. R., Watson A., and Law C. S. (1998) Mixing of a tracer in the pycnocline. *J. Geophys. Res.* **103**(C10), 21499–21529.

Ledwell J. R., Montgomery E. T., Polzin K. L., St. Laurent L. C., Schmitt R. W., and Toole J. M. (2000) Evidence for enhanced mixing over rough topography in the abyssal ocean. *Nature* **403**, 179–182.

Li M. and Garrett C. (1997) Mixed layer deepening due to Langmuir circulation. *J. Phys. Oceanogr.* **27**(1), 121–132.

Li Y.-H., Peng T. H., Broecker W. S., and Ostlund H. G. (1984) The average vertical mixing coefficient for the oceanic thermocline. *Tellus* **36B**, 212–217.

Mackas D. L., Denman K. L., and Bennett A. F. (1987) Least squares multiple tracer analysis of water mass composition. *J. Geophys. Res.* **92**(C3), 2907–2918.

McDougall T. J. (1987) Neutral surfaces in the ocean: implications for modelling. *Geophys. Res. Lett.* **14**(8), 797–800.

McWilliams J. C. (1996) Modelling of the general ocean circulation. *Ann. Rev. Fluid Mech.* **28**, 215–248.

Moore W. S. (1997) High fluxes of radium and barium from the mouth of the Ganges–Brahmaputra rivers during low river discharge suggest a large groundwater source. *Earth Planet. Sci. Lett.* **150**, 141–150.

Moore W. S. (1999) The subterranean estuary: a reaction zone of groundwater and seawater. *Mar. Chem.* **65**, 111–125.

Moore W. S. (2000) Determining coastal mixing rates using radium isotopes. *Continent. Shelf Res.* **20**, 1993–2007.

Morris M. Y., Hall M. M., St. Laurent L. C., and Hogg N. G. (2001) Abyssal mixing in the Brazil basin. *J. Phys. Oceanogr.* **31**, 3331–3348.

Munk W. H. (1966) Abyssal recipes. *Deep-Sea Res.* **13**, 707–730.

Musgrave D. L. (1985) A numerical study of the roles of subgyre-scale mixing and the western boundary current on homgenization of a passive tracer. *J. Geophys. Res.* **90**(C4), 7037–7043.

Musgrave D. L. (1990) Numerical studies of tritium and ^{3}He in the thermocline. *J. Phys. Oceanogr.* **20**, 344–373.

Musgrave D. L., Chou J., and Jenkins W. J. (1988) Application of a model of upper-ocean physics for studying seasonal cycles of oxygen. *J. Geophys. Res.* **93**, 15679–15700.

Okubo A. (1971) Oceanic diffusion diagrams. *Deep-Sea Res.* **18**, 789–802.

Olbers D., Wenzel M., and Willebrand J. (1985) The inference of North Atlantic circulation patterns from climatological hydrographic data. *Rev. Geophys.* **23**, 313–356.

Pickart R. S., Hogg N. G., and Smethie W. M. (1989) Determining the strength of the deep western boundary current using the chlorfluoromethane ratio. *J. Phys. Oceanogr.* **19**(7), 940–951.

Pickart R. S., Smethie W. M., Lazier J. R. N., Jones E. P., and Jenkins W. J. (1996) Eddies of newly formed upper Labrador Sea Water. *J. Geophys. Res.* **101**, 20711–20726.

Polzin K. L., Toole J. M., and Schmitt R. W. (1995) Finescale parametrizations of turbulent dissipation. *J. Phys. Oceanogr.* **25**, 306–328.

Polzin K. L., Toole J. M., Ledwell J. R., and Schmitt R. W. (1997) Spatial variability of turbulent mixing in the abyssal ocean. *Science* **276**, 93–96.

Poole R. and Tomczak M. (1999) Optimum multiparameter analysis of the water mass structure in the Atlantic Ocean thermocline. *Deep-Sea Res.* **46**, 1895–1921.

Quay P., Broecker W. S., Hesslein R. H., and Schindler D. W. (1980) Vertical diffusion rates determined by tritium tracer experiments in the thermocline and hypolimnion of two lakes. *Limnol. Oceanogr.* **25**(2), 201–218.

Redi M. H. (1982) Oceanic isopycnal mixing by coordinate rotation. *J. Phys. Oceanogr.* **12**, 1154–1158.

Rhines P. B. and Young W. R. (1983) How rapidly is a passive scalar mixed within closed streamlines. *J. Fluid Mech.* **133**, 133–145.

Robbins P. E. and Jenkins W. J. (1998) Observations of temporal changes of tritium-^{3}He age in the eastern North Atlantic thermocline: evidence for changes in ventilation? *J. Mar. Res.* **56**, 1125–1161.

Robbins P. E., Price J. F., Owens W. B., and Jenkins W. J. (2000) On the importance of lateral diffusion for the ventilation of the lower thermocline in the subtropical North Atlantic. *J. Phys. Oceanogr.* **30**, 67–89.

Rodgers K. B., Schrag D., Cane M. A., and Naik N. H. (1999) The bomb ^{14}C transient in the Pacific Ocean. *J. Geophys. Res.* **105**(C4), 8489–8512.

Rooth C. G. and Ostlund H. G. (1972) Penetration of tritium into the North Atlantic thermocline. *Deep-Sea Res.* **19**, 481–492.

Sarmiento J. L. and Broecker W. S. (1980) Ocean floor ^{222}Rn standing crops in the Atlantic and Pacific Oceans. *Earth Planet. Sci. Lett.* **49**, 341–350.

Sarmiento J. L. and Biscaye P. (1986) Radon 222 in the Benthic boundary layer. *J. Geophys. Res.* **91**(C1), 833–844.

Sarmiento J. L., Feely H. W., Moore W. S., Bainbridge A. E., and Broecker W. S. (1976) The relationship between vertical eddy diffusion and buoyancy gradient in the deep sea. *Earth Planet. Sci. Lett.* **32**, 357–370.

Sarmiento J. L., Broecker W. S., and Biscaye P. (1978) Excess bottom radon 222 distribution in deep ocean passages. *J. Geophys. Res.* **83**(C10), 5068–5076.

Sarmiento J. L., Rooth C. G., and Broecker W. S. (1982) Radium 228 as a tracer of basin wide processes in the abyssal ocean. *J. Geophys. Res.* **87**(C12), 9694–9698.

Schlitzer R., Roether W., Weidmann U., Kalt P., and Loosli H. H. (1985) A meridional ^{14}C and ^{39}Ar section in the northeast Atlantic deep water. *J. Geophys. Res.* **90**(C4), 6945–6952.

Schlosser P., Bonisch G., Kromer B., Muennich K. O., and Koltermann K. P. (1990) Ventilation rates of waters in the Nansen Basin of the Arctic Ocean derived from a multitracer approach. *J. Geophys. Res.* **C95**, 3265–3272.

Schlosser P., Bonisch G., Rhein M., and Bayer R. (1991) Reduction of deepwater formation in the Greenland Sea during the 1980s: evidence from tracer data. *Science* **251**, 1054–1056.

Schlosser P., Kromer B., Ostlund H. G., Ekwurzel B., Bonisch G., Loosli H. H., and Purtschert R. (1994) On the ^{14}C and ^{39}Ar distribution in the central Arctic Ocean: implications for deep water formation. *Radiocarbon* **36**, 327–343.

Schlosser P. and Smethie W. M. (1995) Transient tracers as a tool to study variability of ocean circulation. In *Natural Variability on Decade-to-Century Time Scales* (ed. N. R. Council). National Research Council, pp. 274–289.

Schlosser P., Bonisch G., Kromer B., Loosli H. H., Buhler R., Bayer R., Bonani G., and Koltermann K. P. (1995a) Mid-1980s distribution of tritium, ^{3}He, ^{14}C, and ^{39}Ar in the Greenland/Norwegian seas and the Nansen basin of the Arctic Ocean. *Prog. Oceanogr.* **35**, 1–28.

Schlosser P., Swift J. M., Lewis D., and Pfirman S. (1995b) The role of large-scale Arctic Ocean circulation on the transport of contaminants. *Deep-Sea Res.* **42**(6), 1341–1367.

Schlosser P., Bullister J. L., Fine R. A., Jenkins W. J., Key R. M., Lupton J. E., Roether W., and Smethie W. M. (2001) Transformation and age of water masses. In *Ocean Circulation and Climate: Observing and Modelling the Global Ocean* (eds. G. Siedler, J. Church, and J. Gould). Academic Press, London, vol. 77, pp. 431–452.

Schmitt R. W. (1981) Form of the temperature-salinity relationship in the central water: evidence for double-diffusive mixing. *J. Phys. Oceanogr.* **11**, 1015–1026.

Schmitt R. W. (1990) On the density ratio balance in the central water. *J. Phys. Oceanogr.* **20**(6), 900–906.

Schmitt R. W. (1994) Double diffusion in oceanography. *Ann. Rev. Fluid Mech.* **26**, 255–285.

Schmitt R. W. (1998) Double-diffusive convection. In *Ocean Modelling and Parametrization* (eds. E. P. Chassignet and J. Verron). Kluwer, Amsterdam, pp. 215–234.

Smethie W. M. (1993) Tracing the thermohaline circulation in the western North Atlantic using chlorofluorocarbons. *Prog. Oceanogr.* **31**, 51–99.

Spitzer W. S. and Jenkins W. J. (1989) Rates of vertical mixing, gas exchange and new production: estimates from seasonal gas cycles in the upper ocean near Bermuda. *J. Mar. Res.* **47**, 169–196.

St. Laurent L. C. and Schmitt R. W. (1999) The contribution of salt fingers to vertical mixing in the North Atlantic tracer release experiment. *J. Geophys. Res.* **29**, 1404–1424.

St. Laurent L. C., Toole J. M., and Schmitt R. W. (2001) Buoyancy forcing by turbulence above rough topography in the abyssal Brazil basin. *J. Phys. Oceanogr.* **31**, 3476–3495.

Stommel H. (1949) Horizontal diffusion due to oceanic turbulence. *J. Mar. Res.* **8**(3), 199–225.

Sundermeyer M. A. and Price J. F. (1998) Lateral mixing and the North Atlantic tracer release experiment: observations and numerical simulations of Lagrangian particles and a passive tracer. *J. Geophys. Res.* **103**(C10), 21481–21497.

Tennekes H. and Lumley J. L. (1972) *A First Course in Turbulence*. MIT Press, Cambridge, MA.

Theile G. and Sarmiento J. L. (1990) Tracer dating and ocean ventilation. *J. Geophys. Res.* **95**, 9377–9391.

Tomczak M. (1999) Some historical, theoretical and applied aspects of quantitative water mass analysis. *J. Mar. Res.* **57**(3), 275–303.

Tomczak M. and Large D. G. B. (1989) Optimum multiparameter analysis of mixing in the thermocline of the eastern Indian Ocean. *J. Geophys. Res.* **94**(C11), 16141–16149.

Toole J. M., Polzin K. L., and Schmitt R. W. (1994) Estimates of diapycnal mixing in the abyssal ocean. *Science* **264**, 1120–1123.

Torgersen T., Turekian K. K., Turekian V. C., Tanaka N., DeAngelo E., and O'Donnell J. (1996) ^{224}Ra distribution in surface and deep water of long island sound: sauces and horizontal transport rates. *Continent. Shelf Res.* **16**(12), 1545–1559.

Unterweger M. P., Coursey B. M., Schima F. J., and Mann W. B. (1980) Preparation and calibration of the 1978

national bureau of standards tritiated-water standards. *Int. J. Appl. Radiat. Isotopes* **31**, 611–614.

Warner M. J. and Weiss R. F. (1985) Solubilities of chlorofluorocarbons 11 and 12 in water and seawater. *Deep-Sea Res.* **32**(12), 1485–1497.

Warner M. J., Bullister J. L., Wisegarver D. P., Gammon R. H., and Weiss R. F. (1996) Basin-wide distributions of chlorofluorcarbons CFC-11 and CFC-12 in the North Pacific, 1985–1989. *J. Geophys. Res.* **101**, 20525–20542.

Weiss W. M. and Roether W. (1980) The rates of tritium input to the world oceans. *Earth Planet. Sci. Lett.* **49**, 435–446.

Young W. R., Rhines P. B., and Garrett C. (1982) Shear-flow dispersion, internal waves and horizontal mixing in the ocean. *J. Phys. Oceanogr.* **12**(6), 515–527.

Zhang R.-H., Rothstein L. M., and Busalacchi A. J. (1998) Origin of upper-ocean warming and El Niño change in decadal scales in the tropical Pacific Ocean. *Nature* **391**, 879–883.

Treatise on Geochemistry
ISBN (set): 0-08-043751-6
Volume 6; (ISBN: 0-08-044341-9); pp. 223–246